Title

Structural insights into substrate recognition by the SOCS2 E3 ubiquitin ligase

Authors

Wei-Wei Kung, Sarath Ramachandran, Nikolai Makukhin, Elvira Bruno, Alessio Ciulli*

Address

Division of Biological Chemistry and Drug Discovery, School of Life Sciences, University of Dundee, James Black Centre, Dow Street, Dundee, DD1 5EH, United Kingdom

Abstract

The suppressor of cytokine signaling 2 (SOCS2) acts as substrate recognition subunit of a Cullin5 E3 ubiquitin ligase complex. SOCS2 binds to phosphotyrosine-modified epitopes as degrons for ubiquitination and proteasomal degradation, yet the molecular basis of substrate recognition has remained elusive. We solved cocrystal structures of SOCS2-ElonginB-ElonginC in complex with phosphorylated peptides from substrates growth hormone receptor (GHR-pY595) and erythropoietin receptor (EpoR-pY426) at 1.98 Å and 2.69 Å, respectively. Both peptides bind in an extended conformation recapitulating the canonical SH2 domain-pY pose, yet capture different conformations of the EF loop via specific hydrophobic interactions. The flexible BG loop, for the first time fully defined in the electron density, does not contact the substrate degrons directly. Cancer-associated SNPs located around the pY pocket weaken substrate-binding affinity in biophysical assays. Our findings reveal insights into substrate recognition and specificity by SOCS2, and provide a blueprint for small molecule ligand design.

* E-mail: a.ciulli@dundee.ac.uk

ORCID ID: 0000-0002-8654-1670

Introduction

Cytokines are small glycoproteins that play important roles in the differentiation, development and function of lymphoid and myeloid cells (Sato and Miyajima, 1994). The Janus kinase (JAK) – signal transducer and activator of transcription (STAT) signaling pathway plays a critical role enabling cells to respond to specific cytokines by regulating gene expression. Suppressor of cytokine signalling (SOCS) proteins, which comprise of cytokine inducible SH2–containing protein (CIS) and SOCS1 – SOCS7, negatively regulate cytokine receptors and inhibit the JAK-STAT signaling pathway (Starr *et al.*, 1997).

SOCS proteins share a conserved domain architecture comprising of an N-terminal extended SH2 subdomain (ESS) that is associates with substrate interaction (Bullock *et al.*, 2006), followed by a central Src-homology 2 (SH2) domain that recognizes a phosphotyrosine (pY) containing sequence (Yoshimura *et al.*, 1995), and a C-terminal SOCS box that interacts with the adaptor ElonginB-ElonginC complex (EloBC) (Kamura *et al.*, 1998, 2004; Zhang *et al.*, 1999). All SOCS proteins bind to EloBC and recruit Cullin5 with high specificity, forming different SOCS-EloBC-Cullin5-Rbx2 ($CRL5^{SOCS}$) E3 ligases that catalyse ubiquitin transfer and subsequent proteasomal degradation of specific substrates, as a mechanism to regulate diverse biological processes (Piessevaux, Lavens, *et al.*, 2008; Babon *et al.*, 2009; Linossi and Nicholson, 2012; Bulatov and Ciulli, 2015). SOCS proteins serve as substrate recognition modules that impart substrate specificity to each $CRL5^{SOCS}$ E3 complex.

Expression of SOCS proteins is induced by cytokine stimulation. Upon cytokine binding to a receptor, receptors oligomerize resulting in activation of the JAK family kinases that phosphorylate specific tyrosine residues on the receptor, including the docking site for the STAT proteins. The docked STAT proteins are sequentially phosphorylated, they dimerize and translocate into the nucleus, initiating gene transcription of several downstream proteins including the SOCS proteins. SOCS proteins suppress the JAK-STAT pathway via three distinct but often concomitant mechanisms: 1) KIR mediated direct JAK inhibition (Sasaki *et al.*, 1999; Yasukawa, 1999); 2) Blocking STAT activation by competing for receptor pY sites (Ram and Waxman, 1999); 3) Targeting the receptor for proteasomal degradation via SOCS E3 ligase activity (Piessevaux, De Ceuninck, *et al.*, 2008; Vesterlund *et al.*, 2011). Some of the SOCS-substrate interactions have been structurally characterized, including SOCS1-JAK (Liau *et al.*, 2018), SOCS3-gp130 (Babon *et al.*,

2006; Bergamin, Wu and Hubbard, 2006), SOCS3-gp130-JAK2 (Kershaw *et al.*, 2013) and SOCS6-cKit (Zadjali *et al.*, 2011).

SOCS2, one of the members of the SOCS family, is implicated in the disorders in immune system, central nervous system and cancer, and is thus emerging as a promising target for cancer therapies (Turnley, 2005; Rico-Bautista, Flores-Morales and Fernández-Pérez, 2006; Haan, 2016; Keating and Nicholson, 2018). SOCS2 has been shown as the primary suppressor of growth hormone (GH) pathway where a gigantism phenotype was observed in a *SOCS2*$^{-/-}$mice (Metcalf *et al.*, 2000). Paradoxically, the SOCS2 overexpressed transgenic mice also led to the same phenotype due to the SOCS2-mediated degradation of SOCS1 and SOCS3 (Greenhalgh, Metcalf, *et al.*, 2002; Tannahill *et al.*, 2005; Piessevaux *et al.*, 2006). Attenuation of GHR signalling relies on two phosphorylation sites at GHR that are recognised by SOCS2 (Greenhalgh *et al.*, 2005; Vesterlund *et al.*, 2011). The pY487 site of GHR interacts with CRL5^{SOCS2} E3 ligase that targets the GHR for ubiquitination and proteasomal degradation (Vesterlund *et al.*, 2011). A downstream pY595 site interacts with SOCS2, STAT5b and SHP2 (SH2 domain-containing phosphatase 2), enabling SOCS2 to inhibit the signaling by blocking this receptor site from STAT5b (Hansen *et al.*, 1999; Ram and Waxman, 1999; Stofega *et al.*, 2000; Greenhalgh, Bertolino, *et al.*, 2002). Nonetheless, deletion of both sites is required to remove the inhibitory effect of SOCS2 on the GH signaling (Greenhalgh *et al.*, 2005; Vesterlund *et al.*, 2011). Analysis of the binding affinity of SOCS2 for these two phosphorylation sites of GHR reveals that the pY595 region exhibits a higher affinity towards SOCS2 (K_D = 1.6 μM) compared to pY487 region (K_D = 11.3 μM) (Bullock *et al.*, 2006, 2007; Bulatov *et al.*, 2015). An 11-mer phosphorylated peptide spanning the pY595 region of GHR was sufficient to pull down the whole CRL5^{SOCS2} complex from human cell lysates (Bulatov *et al.*, 2015). as well as CIS, the closest homologue to SOCS2 from the same family, which plays a role in anti-tumor immunity controlling the differentiation of CD4 T helper cell, and the IL-2 and IL-4 response (Yang *et al.*, 2013; Bulatov *et al.*, 2015). In addition to GHR and CIS, other substrates have been identified to interact with SOCS2, including the erythropoietin receptor (EpoR) at pY426 (Eyckerman *et al.*, 2001), the leptin receptor at pY1077 (Lavens, 2006), the epidermal growth factor receptor (Goldshmit *et al.*, 2004) and the insulin-like growth factor-I receptor (Dey *et al.*, 1998). The first crystal structure of SOCS2-ElonginB-ElonginC (SBC) was reported in 2006 (Bullock *et al.*, 2006), however the structural basis for substrate recognition to SOCS2 has yet remained elusive.

99 Here, we determine the first co-crystal structures of SBC in complex with phosphorylated
100 epitope peptides from its physiological targets GHR and EpoR. Our structures reveal the
101 peptides are accommodated in an extended conformation to capture specific interactions
102 with SOCS2. A key flexible region of SOCS2, known as the BG loop, is defined in the
103 electron density for the first time and shown not to contact the bound substrates. Structural
104 analyses supported by biophysical and mutagenesis investigations allowed identification of
105 hotspot residues on the substrate degrons and functional elucidation of disease-relevant
106 single nucleotide polymorphisms (SNPs) of SOCS2. Our findings provide fresh insights
107 into the molecular recognition and selectivity between SOCS2 and target substrates, and
108 provide an important template for future structure-guided ligand design.
109
110 **Results**
111 To elucidate the molecular basis of substrate recognition by SOCS2, we subjected the
112 SOCS2-ElonginB-ElonginC (SBC) complex to extensive co-crystallization trials with 11-
113 residue phosphopeptides of either EpoR or GHR that span the regions surrounding Tyr426
114 and Tyr 595 region, respectively. The affinity of SBC for EpoR_pY426 (K_D of 4.8 μM) and
115 GHR_pY595 (K_D of 1.6 μM) was measured by isothermal titration calorimetry (ITC), and
116 found to be consistent with the literature (Bullock *et al.*, 2006; Bulatov *et al.*, 2015) (Figure
117 S1). Attempts to co-crystallize wild-type SBC protein constructs (Bullock *et al.*, 2006;
118 Bulatov *et al.*, 2015) with either GHR or EpoR peptide were unsuccessful as resulting
119 crystals only diffracted poorly. To improve crystal quality, we engineered a cluster of three
120 mutations K115A/K117A/Q118A on SOCS2 that was predicted to significantly reduce
121 surface conformational entropy and thermodynamically favor crystal packing (Goldschmidt
122 *et al.*, 2007). Crystallization attempts with this new $S^{KKQ}BC$ triple-mutant construct
123 (K115A/K117A/Q118A on SOCS2) eventually yielded high-resolution datasets.
124
125 *SBC-EpoR co-crystal structure*
126 The structure of SBC in complex with EpoR_pY426 peptide (SBC-EpoR) was solved and
127 refined at 2.69 Å with 19.64 % R_{work} and 23.51 % R_{free} (Table 1). The overall subunit and
128 domain arrangements of the SBC-EpoR structure is consistent with those of the apo SBC
129 structures (Bullock *et al.*, 2006; Kim *et al.*, 2013; Gadd, Bulatov and Ciulli, 2015) (Figure
130 1a). Electron density for nine out of eleven non-terminal EpoR_pY426 residues are well
131 defined in the structure (Figure 1b). A classic SH2 domain-pY peptide interaction is
132 observed where the pY residue is anchored at the pY pocket and the flanking residues are
133 extending across the SH2 domain. The pY residue is tightly locked by an intricate

hydrogen-bonding network formed by residues Arg73, Ser75, Ser76, Thr83 and Arg96 of SOCS2 (Figure 1c). Additional hydrogen bonds are formed along the backbone of EpoR_pY426 peptide from Glu(-1) to Leu(+3) with SOCS2 residues Thr93, Asn94, Asp107 and one structural water (Figure 1d). Multiple hydrophobic interactions also support the binding of EpoR_pY426 C-terminal residues, Ile(+2), Leu(+3) and Pro(+5) that are well accommodated within a hydrophobic patch created by Leu95, Leu106, Ser108, Ile109, Val112, Leu116 and Leu150 of SOCS2 (Figure 1e).

Crystal structure of SBC-GHR

Encouraged by the success in solving an SBC-EpoR structure, to deepen understanding of the SOCS2 binding epitopes, we co-crystallized SBC with an 11-mer GHR_pY595 peptide (SBC-GHR) and solved the structure at 1.98 Å resolution with 21.73 % R_{work} and 24.08% R_{free} (Table 1). In contrast to SBC-EpoR, which contains one protomer in the asymmetric unit, the SBC-GHR contains two copies of protomer. Alignment of these two protomers via the backbone atoms of the EloB subunit reveals a hinge motion between the SH2 domain and the SOCS box (Figure S2). Such motion is a common feature in SOCS box and F-box containing proteins and it has been shown to be important as it facilitates accurate orientation and positioning of a target substrate protein relative to the multisubunit CRL complex (Liu and Nussinov, 2009; Gadd, Bulatov and Ciulli, 2015). Contrary to the SBC-EpoR complex, which contains a single copy of peptide per SH2 domain, two copies of GHR_pY595 peptides were found binding per SH2 domain of SOCS2 (giving a total of four copies within the asymmetric unit). The two peptides run in an anti-parallel direction relative to each other across the SH2 domain, with well-defined electron density surrounding them both (Figure 2a). One of the peptides (referred to as peptide A hereafter) binds to SH2 domain in a canonical manner, where the pY is recognized by the positively charged pY pocket between the central β strands and αA (Figure 2b). In contrast, the second peptide, peptide B, has its pY residue exposed to solvent and interacting only with His149 of SOCS2 (Figure 2b).

Specific interaction of the GHR_pY595 phosphopeptide

The unusual simultaneous binding observed for the GHR substrate peptide to SOCS2 SH2 domain is imparted mainly by the region comprising Ser(+2) to Val(+6) from each peptide, which pair such that they form an anti-parallel beta sheet (Figure 2c). Extensive hydrogen bonds are formed between the backbone of the two peptides and backbone residues of SOCS2 and structural waters (Figure 2c). Further hydrophobic interactions

appear to reinforce the binding, which impart specificity for GHR. The Ile(+3) and Ile(+5) of peptide A and peptide B settle in a hydrophobic patch of the SH2 domain formed by Leu95, Leu106, Ser108, Leu116 and Leu150 (Figure 2d). Another hydrophobic interaction that is distinct in SBC-GHR compared to SBC-EpoR is that formed by the side chain of Val(-3) of peptide A, that nicely fits into a hydrophobic pocket comprising of Thr88, Ala90, Thr93, Leu95 and Val148 from SOCS2 (Figure 2e). In the SBC-GHR structure, a cobalt ion is modeled at a positive peak that disappeared only at 21 σ level in the unbiased Fo-Fc electron density map. This cobalt ion satisfies the formation of an octahedral coordination geometry with the side chains of His(+4) of peptide B, His149 of SOCS2 and with three surrounding water molecules (Figure 2f).

The BG loop of SOCS2 is observed for the first time in an open conformation

SOCS2 is known to recognize two GHR binding sites at regions around pY487 and pY595, respectively. We therefore hypothesized that the two copies of the GHR peptides bound in the crystal structure might mimic a physiological folded conformation of GHR, presenting each of the phosphorylated sites bound simultaneously to SOCS2 (Figure 3a). To test this hypothesis, we utilized an 11-residue GHR_pY487 phosphopeptide (NIDFpYAQVSDI, K_D of 2.5 μM by SPR), mixed with the GHR_pY595 peptide and SBC in equimolar 1:1:1 ratio for co-crystallization. In this crystal structure (hereafter referred to as SBC-GHR_2), still two copies of the GHR_pY595 peptide, but no GHR_pY487, are observed bound, yielding a structure very similar to the previous SBC-GHR structure (Figure 3b). However, an important observation and different in SBC-GHR_2 compared to our other co-crystal structures was that the regions of SOCS2 corresponding to residues 134-162 is now fully visible in the electron density. This is unprecendented, and the first time this region, also called BG loop is structurally defined in full. The BG loop connects the βE and βF strands of an SH2 domain (Figure 4a). The first part of the BG loop (residues 134-148 in SOCS2) differs in length and sequence among SOCS proteins (Figure 4b). We refer herein to this more variable region as the “specificity BG loop”, because its conformation, together with the configuration of the adjacent EF loop, governs accessibility of the pY binding pocket and contributes to substrate specificity in SH2 domains (Kaneko *et al.*, 2010). A particular region in the middle of the specificity BG loop (residues 136-145) is found to be disordered in all previously determined SOCS2 structures (PBD code, 2C9W, 4JGH and 5BO4) as well as our other co-crystal structures SBC-GHR and SBC-EpoR. In this SBC-GHR_2 structure, the BG loop is in an open conformation stabilised by crystal contacts, Pro140

203 (BG loop) to Arg186 (SOCS box) and Pro140 (BG loop) to Ile90 (EloB), as clearly defined
204 by the unbiased omit map at this region (Figure 4c, Table 1).
205
206 *Conformational changes of the EF and BG loop*
207 The configuration of the EF and BG loops play an important role in governing the
208 accessibility of the binding pocket and specificity toward ligand binding (Kaneko *et al.*,
209 2010). A comparison of the SOCS2 structures in the presence and absence of peptides
210 bound highlight conformational changes in EF (residue 107-116) and BG loop. In the
211 absence of substrate peptide, the EF loop curls up placing the Ile110 and Cys111 at the
212 hydrophobic SH2 domain (Figure 5a). Upon binding of a substrate peptide, the EF loop
213 opens up forming backbone interactions with GHR_pY595 (Figure 5b), or rearranges itself
214 to allow a specific interaction with EpoR_pY426 (Figure 5c). This specific interaction
215 between EF loop and EpoR_pY426 involves hydrophobic interactions between Ile109 and
216 Val112 of SOCS2, Val112 of a SOCS2 symmetry mate, and Pro(+5) of EpoR_pY426,
217 resulting in a differential binding mode from GHR_pY595 to SOCS2. The BG loop of
218 SOCS2 is observed to be in an open conformation in SBC-GHR_2 and SBC-EpoR
219 (disordered) structures. A superimposition of the two substrate complex structures suggest
220 that the BG loop opens up further in SBC-GHR structure to accommodate two GHR
221 peptides (Figure 5d).
222
223 *Biophysical characterization of specificity between GHR_pY595 and SOCS2*
224 To evaluate the specificity of the protein-peptide interaction in solution, we designed
225 single-point mutations on the peptide first, and compared their binding to wild-type peptide
226 by two orthogonal biophysical methods: a direct binding assay using SPR (SBC
227 immobilized on the chip) and ^{19}F ligand-observed displacement NMR assays. In the ^{19}F
228 NMR displacement assay, the fluorine signal of a purposely-designed reporter ligand (also
229 referred to as spy molecule) was monitored as a mean to quantify the extent of the
230 competition between the tested peptides and the spy molecule. A Carr-Purcell-Meibom-Gill
231 (CPMG) pulse sequence was applied to estimate the spin-spin relaxation time (T_2) of the
232 spy molecule in the absence and presence of protein (Carr and Purcell, 1954; Meiboom,
233 Gill and Gillt, 1958; Dalvit *et al.*, 2003). By adding competitor to disrupt the protein-spy
234 interaction, the binding affinity of a competitor can be calculated based on the degree of
235 displacement of the spy (Wang, Liu and Wyss, 2004). The spy molecule used in our assay
236 is phosphate **3**, a fluorinated pY analogue that specifically binds to the pY pocket with a K_D

237 of 40 μM (Scheme 1, and Figure S3). The two assays were found to be robust and reliable
238 and measured K_d values to correlate very well (Figure S4)
239
240 First, we focused on the unique interaction formed by Val(-3) of GHR_pY595, which
241 inserts into a small hydrophobic cavity of SOCS2 (Figure 2e). This interaction was
242 investigated by mutating Val(-3) in the GHR peptide to Tyr and Arg, as representative
243 bulky and charged residues, respectively. We hypothesized this structural change would
244 disrupt the fit at this small hydrophobic pocket. Mutant V(-3)R exhibited between a 7- and
245 a 10-fold loss of binding affinity to SBC, depending on the assay, suggesting the charged
246 group strongly disrupts the interaction (Table 2). By contrast, the V(-3)Y was less
247 disruptive, with only a two-fold loss in affinity.
248 Next, to map the relative importance and contribution of each individual amino acids to the
249 binding affinity with SBC, alanine scan of the substrate peptides was invoked. The peptide
250 sequences were designed such that individual amino acids were separately mutated into
251 alanine except pY, which is known to abolish binding if mutated even to unphosphorylated
252 Y (Bulatov *et al.*, 2015). The resulting library comprised of the original wild-type
253 sequences, ten derivatives from GHR_pY595 and nine from EpoR_pY426, and was
254 characterized in parallel using SPR and ^{19}F NMR competition assay (Table 3). Alanine
255 substitution at pY(-3), pY(-1), pY(+3) and pY(+4) of the GHR_pY595 resulted in at least
256 two-fold weakened binding (increase in K_D) compared to the wild type. In contrast, a
257 similar 2-fold weakening in binding affinity was observed in the EpoR_pY426 peptide upon
258 alanine substitution at pY(-1), pY(+2) and pY(+3). These results are consistent with
259 observations from our crystal structures that peptide-SOCS2 binding is mediated by
260 hydrophobic interaction including pY(-3), pY(+3) and pY(+5) on the GHR_pY595 and
261 pY(+2) and pY(+3) on the EpoR_pY426. The binding affinity for each peptide also dropped
262 by at least two-fold with Ala substitution at pY(-1) position, indicating the importance of the
263 residue just upstream of pY.
264
265 *SNPs study*
266 Several single nucleotide polymorphisms (SNPs) on SOCS2 are reported in the Catalogue
267 of Somatic Mutation in Cancer database (COSMIC) as potentially linked to cancers such
268 as tumours of the lung, breast, and pancreas (Forbes *et al.*, 2017). We thus next decided
269 to characterize the interaction of selected SNP SOCS2 mutants with substrate peptides
270 GHR_pY595, EpoR_pY426 and GHR_pY487 by SPR. Inspection of our SBC co-crystal
271 structures guided us to select five known SNPs: N94D, R96L, R96Q that are located in the

pY-pocket and involved in direct recognition of pY; L106V that is highly conserved at the hydrophobic SH2 domain involving in substrate interaction; and C133Y that participates in the SH2 hydrophobic core (Figure 6a). All mutant proteins expressed and purified similarly to wild-type, and the mutations did not appear to affect the structural integrity and solubility of the constructs, as observed by ^{1}H NMR (Figure S5).

The L106V and C133Y mutations did not affect binding affinities except to the GHR_pY487 peptide for which a 2-fold weaker binding was observed compared to wild type (Figure 6b). In contrast, the N94D and R96L mutations drastically impaired substrate binding, leading to almost undetectable binding response by SPR. Because of the low signal-to-noise, reliable K_D values could not be measured with these protein mutants. For the R96Q mutation no signal response was detected, suggesting that binding was completely abolished and highlighting the most disruptive of the mutations studies. In addition to SPR, the SNP mutants were characterized using ^{19}F NMR by monitoring the signal contrast in the presence and absence of protein. L106V and C133Y exhibited similar contrast, 67% and 77%, comparable to wild type at 69 %, suggesting these mutations did not affect pY recognition. Mutations on N94 and R96 showed a substantial disruption to pY recognition, resulting in a significant disruption of binding at around 20% contrast. Strikingly, the R96Q completely abolished binding, consistent with the SPR data (Figure 6c).

Discussion

SOCS2 is a substrate binding protein of the CRL5 E3 complex that negatively regulates the JAK-STAT signaling by targeting substrate receptors for degradation and blocking STAT5b activation by competing with receptor pY sites. The details of these interactions have remained elusive and to date structural information remained limited to apo SOCS2. Herein, we have disclosed two novel structures of the SBC in complex with substrate peptides EpoR_pY426 and GHR_pY595. Both peptides recapitulate a canonical substrate-binding mode to SH2 domain of SOCS2, but catch different hydrophobic interactions resulting in exclusive binding modes with distinct hydrophobic cavities in SOCS2.

The BG loop of SOCS2 had not been fully revealed in previous published structures. Here, we report an open conformation BG loop, which is contradictory to other SOCS structures with bound peptides, for example SOCS3:gp130 and SOCS6:c-kit (Bergamin, Wu and Hubbard, 2006; Zadjali *et al.*, 2011). In the SOCS3 and SOCS6 peptide-bound structures, the BG loop folds up as a hairpin interacting with the substrate peptide, forming a triple-stranded β sheet structure (Figure 7a,b). The corresponding BG loop region in SOCS2 is either fully disordered or in an open conformation (SBC-EpoR and SBC-GHR_2), suggesting that this region does not participate in substrate recognition. Nevertheless, interestingly, a similar triple-stranded β sheet structure is observed in the SBC-GHR_2 structure, where the peptide B replaces the first β-sheet of the BG loop and makes backbone interactions with BG loop (Val148 and Leu150) and peptide A (Ser(+2) to Val(+6)) (Figure 7c).

The BG loop along with the EF loop forms a hydrophobic channel in SOCS3 and SOCS6. This channel imparts specificity and restricts the binding of substrates. In contrast the open conformation of BG loop in SOCS2 could be critical in enabling SOCS2 to accommodate a wider range of substrates including GHR, EpoR, SOCS1 and SOCS3 amongst others. A comparison of buried surface area of the substrate peptides among SOCS proteins, reveal that EpoR and GHR binds with SOCS2 with only 595 and 641 $Å^2$, respectively, in contrast to areas of 1714 $Å^2$ for SOCS6/c-KIT and 1761 $Å^2$ for SOCS3/gp130 complexes. Unlike SOCS3 and SOCS6 complex structures, the pY flanking residues from EpoR and GHR do not participate in extensive side-chain hydrogen bonding interactions. Together, these observations are consistent with greater binding affinities of SOCS3 and SOCS6 substrates compared to SOCS2 substrates. The lower potency of affinity for SOCS2 substrates could contribute to its relatively greater promiscuity to multiple substrates.

The observation of the dual-peptide binding mode to SOCS2 was unexpected, however is not unprecedented with SH2 domains, as reported previously with the tyrosine phosphatase SHP-2, which also contains a SH2 domain (Zhang *et al.*, 2011). In the co-crystal structure of SHP-2:pY peptide solved by Zhang et al., one pY of the peptide is recognized at the pY pocket and the other one is solvent exposed as in our structures described herein. Besides, two peptides run antiparallel to each other and form an antiparallel four-stranded β sheet with BG loop. Zhang *et al*. suggested that the dimerization of peptide binding in SHP-2 requires at least one pY containing peptide and demonstrates enhanced binding affinity to protein. For our SBC-GHR structure, despite preparing several protein-peptide samples for co-crystallization at 1:1 molar ratio, all dataset collected from crystals were consistent with a 1:2 (protein-peptide) binding mode. Two hypotheses are proposed to explain this observation of the dual-peptide binding. In one hypothesis, the substrate might fold back as a hairpin structure presenting a new binding epitope for recognition, thus adding an extra layer of selectivity to signaling. Alternatively, in a second hypothesis, SOCS2 might play a role as scaffold bringing two substrates in close proximity, for example by recruiting one instance of phosphorylated substrate to assist the binding of un-phosphorylated one for post-translational modification. This mechanism evokes potential similarities with some phosphodegrons which require two sites to be phosphorylated, utilizing a first kinase to “prime” phosphorylation events, followed by a second kinase for follow-on phosphorylation (Mészáros *et al.*, 2017). An example of such a mechanism is the β-catenin degradation mediated by the β-TrCP (Liu *et al.*, 2002). Further biophysical investigation is warranted to address the extent to which these potential mechanisms might be invoked for SOCS2 function.

SOCS2 is an attractive therapeutic target due to its links to cancer, diabetes, neurological and inflammatory diseases (Alexander and Hilton, 2004; Turnley, 2005; Yoshimura, Naka and Kubo, 2007; Inagaki-Ohara *et al.*, 2013; Linossi *et al.*, 2013; Galic *et al.*, 2014; Keating and Nicholson, 2018). Breast, lung, liver and ovarian cancer have been correlated with down-regulation in SOCS2 (Wikman *et al.*, 2002; Sutherland *et al.*, 2004; Farabegoli *et al.*, 2005; Haffner *et al.*, 2007; Qiu *et al.*, 2013; Zhu *et al.*, 2013). In addition to the JAK-STAT pathway, a recent study has identified the involvement of SOCS2 in the NF-κB (nuclear factor kappa-light-chain-enhancer of activated B cells) pathway that regulates the immune and inflammatory responses (Oeckinghaus and Ghosh, 2009; Paul *et al.*, 2017). NF-κB is found to be constitutively activated in many types of cancer and influences a diverse array

363 of pro-tumorigenic functions, therefore NK-κB plays an pivotal role in cancer initiation and
364 progression (Hoesel and Schmid, 2013). SOCS2 negatively regulates TNFα induced NF-
365 κB activation by targeting NDR1, a serine-threonine kinases, for proteasomal degradation.
366 Hence SOCS2 deficiency may lead to an increased level of NDR1, which was is reported
367 to result in aggressive behaviour of PC3 prostate cancer cells (Paul *et al.*, 2017). These
368 evidences highlight the potential in targeting SOCS2 for drug discovery for inflammation
369 and cancer biology. We have revealed structural insights into the SOCS2-peptide
370 interactions by X-ray crystallography and identified hotspot using alanine scanning,
371 mutation study and SNPs study. This information provides a template to guide the
372 structure-based rational design of SOCS2 ligands that are instrumental in the development
373 of novel chemical tools to address biological question of SOCS2, and in the quest for
374 novel small molecule ligands binding to SOCS2 as potential therapeutics. SOCS2 binders
375 at the pY binding pocket can be used as inhibitors of the $CRL5^{SOCS2}$, which would be
376 expected to prevent degradation of target substrate receptors, thus prolonging the activity
377 of cytokine signaling pathway and upregulating expression of endogenous STAT5b-
378 responsive gene expression. In a distinct application, a SOCS2 binder could be used as
379 E3 ligase ligand handle for designing new chemical degraders to hijack SOCS2 CRL
380 activity and trigger the degradation of unwanted proteins inside cell (Hughes and Ciulli,
381 2017; Lucas and Ciulli, 2017; Ottis and Crews, 2017). This approach, also known as
382 proteolysis targeting chimeras (PROTACs), offers the advantage of inducing rapid and
383 selective intracellular depletion of the target protein, as opposed to mere blockade of a
384 single interaction or activity, which pairs more closely to genetic target validation and often
385 results in greater maximal efficacy of intervention in a signaling pathway. PROTAC-
386 mediated protein degradation has been shown to occur at very low compound
387 concentration (pM to nM range) also potentially allows targeting of intractable protein
388 targets that are beyond the reach of conventional small-molecule approaches that require
389 full occupancy of a target binding site e.g. receptor antagonists and enzyme inhibitors. A
390 limited set of E3 ligases have been targeted so far for PROTACs, notably VHL (Zengerle,
391 Chan and Ciulli, 2015; Maniaci *et al.*, 2017) and cereblon (Lu *et al.*, 2015; Winter *et al.*,
392 2015)(REFs), so extending the approach to other ligandable E3 ligases would be an important
393 advance to the field. Our peptide-bound co-crystal structures suggest that SOCS2 might be
394 ligandable and provide a blueprint for the rational structure-guided design of novel SOCS2
395 inhibitors and SOCS2 ligand handles for PROTACs.
396
397

Materials and Methods

Cloning and protein expression

The human SOCS2 (amino acids 32 – 198) and the ElonginB (amino acids 1 – 104) and ElonginC (amino acids 17 – 112) plasmids were used for protein expression as previously reported (Gadd, Bulatov and Ciulli, 2015), and as templates for mutagenesis. SOCS2 mutants with N94D, R96L, R96Q, L106V or C133Y mutation were introduced using a PCR-based method site-directed mutagenesis. SOCS2 wild type and mutants were co-expressed and purified as previously described (Bulatov *et al.*, 2015; Gadd, Bulatov and Ciulli, 2015).

Crystallization and structure determination of SBC-GHR

To improve crystallization, surface entropy reducing mutations were introduced into SOCS2 construct (amino acids 32 – 198). Three mutation clusters (K63A/E64A/E67A; K113A and K115A/K117A/Q118A) were identified with the SER server (Goldschmidt *et al.*, 2007). SER-assisted crystallization attempts yielded crystals with the K115A/K117A/Q118A SOCS2-EloBC (S^{KKQ}BC). Five times molar excess of GHR_pY595 (PVPDpYTSIHIV-amide) was incubated with S^{KKQ}BC, followed by removing unbound peptide using a protein concentrator. Sample was concentrated to 22 mg/ml with an additional 0.1 M of sodium cacodylated pH7.2 added to the sample. Diffraction-quality crystals were obtained with 0.005 M Cobalt (II) choride, 0.1 M MES pH 6.5, 1.0 M ammonium sulphate at 4 °C using hanging drop vapour diffusion method at 2:1 protein:precipitant ratio. Crystals were cryo-protected using 20% MPD prior to vitrification in liquid nitrogen.

Diffraction data were collected at 100 K at Diamond Light Source beamline i04 using Pilatus 6M-F detector at 0.98 Å wavelength. Indexing and integration was processed by XDS (Kabsch, 2010) and scaling and merging with AIMLESS within the CCP4 program suite (Winn *et al.*, 2011; Evans and Murshudov, 2013). The experimental phases was obtained by identifying positions of arsenic atom using MR-SAD Phases in the PHENIX software suite (McCoy, Storoni and Read, 2004; McCoy *et al.*, 2007) with a model provided. The provided template was a lower resolution SBC-GHR co-crystal obtained previously (unpublished work). The structure was reconstructed by AutoBuild (Terwilliger *et al.*, 2007; Adams *et al.*, 2010) and manually built in Coot (Emsley *et al.*, 2010). The resulting structure was refined iteratively with REFMAC5 (Murshudov *et al.*, 2011)

433 *Crystallization and structure determination of SBC-EpoR*

434 Five times molar excess of EpoR_pY426 (ASFEpYTILDPS-amide) was incubated with
435 $S^{KKQ}BC$ (5mg/ml). Unbound peptide was removed by a protein concentrator (sartorius
436 Vivaspin) while the mixture was concentrated to 20 mg/ml concentration. Sodium
437 cacodylate pH7.2 was added to a final concentration of 0.1M prior to crystallisation.
438 Crystallisation drops were set up in a ratio of 1:1 protein:precipitant in 18% ethanol, 0.1M
439 HEPES pH7.5, 0.1M $MgCl_2$ using hanging drop at 4°C. Crystals were cryo-protected using
440 20 % PEG400 prior to flash-cooled.

441

442 Diffraction data were collected at 100 K on beamline i24 at Diamond Light Source. Data
443 were recorded to Pilatus3 6M-F detector at 0.97 Å wavelength. Data were indexed,
444 integrated, and reduced using XDS (Kabsch, 2010) and AIMLESS (Winn *et al.*, 2011;
445 Evans and Murshudov, 2013). The phase was obtained by molecular replacement (MR)
446 using Phaser (McCoy *et al.*, 2007) with the coordinates of SOCS2-EloB-EloC (PBD ID:
447 2C9W) as a search model. The presence of the EpoR_pY426 was observed in the initial
448 electron density map. Model building was conducted manually with Coot (Emsley *et al.*,
449 2010) and refined with cycles of retrained refinement with REFMAC5 (Murshudov *et al.*,
450 2011).

451

452 *Crystallization and structure determination of SBC-GHR_2*

453 GHR_pY595 (PVPDpYTSIHIV-amide) and GHR_pY487 (NIDFpYAQVSDI-amide) were
454 mixed with $S^{KKQ}BC$ at 1:1:1 stoichiometric ratio with a final concentration of 20 mg/ml and
455 additional 0.1 M sodium cacodylate pH7.2. Drops of the complex were mixed 2:1 with
456 0.005 M cobalt chloride, 0.1 M MES pH6.5 and 1.0 M ammonium sulphate in the sitting-
457 drop vapor diffusion format at 4°C. 20 % MPD was applied to crystal before flash-cooling.

458

459 Data collection of the SBC-GHR_2 co-crystal was at 100 K on beamline i24 at Diamond
460 Light Source. Images were indexed, intergraded and reduced using XDS (Kabsch, 2010)
461 and AIMLESS (Winn *et al.*, 2011; Evans and Murshudov, 2013). A molecular replacement
462 solution was obtained by Phaser (McCoy *et al.*, 2007) using SBC-GHR as search model.
463 Refinement was performed using REFMAC5 (Murshudov *et al.*, 2011) and model building
464 was performed in COOT (Emsley *et al.*, 2010).

465

466 *Synthetic details*

All chemicals, unless otherwise stated were commercially available and used without further purification. Solvents were anhydrous and reactions preformed under positive pressure of nitrogen. Flash column chromatography was performed using a Teledyne Isco Combiflash Rf or Rf200i. As prepacked columns RediSep Rf Normal Phase Disposable Columns were used. NMR spectra were recorded on a Bruker 500 Ultrashield. ^{13}C spectra were ^{1}H decoupled. Chemical shifts (δ) are reported in ppm relative to solvent (CD_3OD: δ_H = 3.31ppm, δ_C = 49.0 ppm) as internal standard. Low resolution MS and analytical HPLC traces were recorded on an Agilent Technologies 1200 series HPLC connected to an Agilent Technologies 6130 quadrupole LC/MS, connected to an Agilent diode array detector. The column used was a Waters XBridge column (50 mm × 2.1 mm, 3.5 µm particle size) and the compounds were eluted with a gradient of 5−95% acetonitrile/water + 0.1% formic acid over 3 min. Preparative HPLC was performed on a Gilson Preparative HPLC System with a Waters X-Bridge C18 column (100 mm x 19 mm; 5 µm particle size) and a gradient of 5 % to 95 % acetonitrile in water over 10 min, flow 25 mL/min, with 0.1 % formic acid in the aqueous phase.

Cbz-O-bis(dimethylamino)phosphono)-L-tyrosine (**1**)

O-bis(dimethylamino)phosphono)-*L*-tyrosine (Chao *et al.*, 1995) (485 mg, 1.54 mmol) and $NaHCO_3$ (260 mg, 3.1 mmol) were dissolved in the mixture THF/H_2O = 1:1 (10 mL) and *N*-(benzyloxycarbonyloxy)succinimide (383 mg, 1.54 mmol) was added. The reaction mixture was stirred at room temperature overnight. After the addition of 5% $NaHSO_4$ the product was extracted with ethyl acetate, washed with brine, dried over $MgSO_4$, concentrated by rotary evaporation under reduced pressure. After drying, Cbz-*O*-bis(dimethylamino)phosphono)-*L*-tyrosine **1** (620 mg, 89%) was obtained as pale yellow. ^{1}H NMR (CD_3OD): 2.69 (d, J = 10.1 Hz, 12H), 2.92 (dd, J = 14.0, 9.3 Hz, 1H), 3.18 (dd, J = 14.0, 4.9 Hz, 1H), 4.40 (dd, J = 4.9, 9.3 Hz, 1H), 5.03 (s, 2H), 7.06 (d, J = 8.5 Hz, 2H), 7.21 (d, J = 8.5 Hz, 2H), 7.25-7.36 (m, 5H). ^{31}P NMR (CD_3OD): 18.2.

(S)-2-amino-3-(4-((bis(dimethylamino)phosphoryl)oxy)phenyl)-N-methylpropanamide (**2**)

To a mixture of the compound **1** (160 mg, 0.35 mmol), HATU (135 mg, 0.35 mmol), HOAt (48 mg, 0.35 mmol) and DIPEA (150 µL, 1 mmol) in DMF (1 mL), 2M methylamine solution in THF (0.5 mL) was added under stirring at room temperature. After two hours, LC-MS analysis showed complete conversion of the starting material and formation of the desired product. The mixture was diluted with ethyl acetate, washed with 5% $NaHSO_4$, brine, dried over $MgSO_4$, concentrated by rotary evaporation under reduced pressure. The crude

product was dissolved in the mixture ethanol/ethyl acetate= 1:1 (8 mL). Hydrogenation was carried out using H-Cube at 80 ˚C, Pd/C, 1 atm, at 1mL/min. The solvent was evaporated under vacuum to afford **2** (108 mg, 92%) which was directly used in the next step without any further purification. ^{1}H NMR (CD_3OD): 2.66 (s, 3H), 2.71 (d, *J* = 10.1 Hz, 12H), 2.81 (m, 1H), 2.96 (m, 1H), 3.51 (m, 1H), 7.09 (dd, *J* = 8.5, 1.0 Hz, 2H), 7.20 (d, *J* = 8.5 Hz, 2H). ^{31}P NMR (CD_3OD): 18.3.

(S)-4-(3-(methylamino)-3-oxo-2-(2,2,2-trifluoroacetamido)propyl)phenyl dihydrogen phosphate (**3**)

A solution of the compound **2** (80 mg, 0.24 mmol) and DIPEA (85 µL, 0.48 mmol) in DCM (2 mL) was cooled to -78 °C, and trifluoroacetic anhydride (34 µL, 0.24 mmol) was added. The reaction mixture was stirred 1h at -78 °C. After solvent evaporation the residue was dissolved in acetonitrile (0.5 mL) and 2M HCl was added (2 mL). The mixture was stirred at room temperature overnight until no presence of the starting materials was detected by LC-MS. The solvents were evaporated and residue was purified by HPLC to afford phosphate **3** (30 mg, 34%) as a white solid. ^{1}H NMR (CD_3OD): 2.69 (s, 3H), 2.96 (dd, *J* = 13.8, 6.4 Hz, 1H), 3.15 (dd, *J* = 13.8, 6.4 Hz, 1H), 4.57 (dd, *J* = 8.8, 6.4 Hz, 1H), 7.13 (dd, *J* = 8.5, 1.1 Hz, 2H), 7.22 (d, *J* = 8.5 Hz, 2H). ^{13}C NMR (CD_3OD): 26.3, 37.8, 56.5, 117.3 (q, *J* = 286.7 Hz), 121.3 (d, *J* = 4.5 Hz), 131.3, 134.1, 151.9 (d, *J* = 6.8 Hz), 158.7 (q, *J* = 37.5 Hz), 172.4. ^{31}P NMR (CD_3OD): 3.7. ^{19}F NMR (CD_3OD): -75.6.

Peptide synthesis

All peptides were prepared via solid-phase peptide synthesis on 10 mmol scale using standard Fmoc chemistry on Rink amide resin (0.68 mmol/g) on an INTAVIS ResPepSL automated peptide synthesizer. *O*-(dibenzylphosphono)-*N*-Fmoc-*L*-tyrosine was synthesised as described below. The peptides were cleaved with 2.5% triisopropylsilane and 2.5% water in TFA. The crude peptides were isolated from the cleavage mixture by precipitation with cold ether, dissolved in the mixture water/DMF=1/1 and purified by preparative HPLC under the following conditions: Waters X-Bridge C18 column (100 mm x 19 mm; 5 µm particle size), gradient of 5-95 % acetonitrile in water over 10 min, flow 25 mL/min, with 0.1 % formic acid in the aqueous phase, UV detection at λobs = 190 and 210 nm). The poor soluble peptides were purified according to the literature procedure (Biosystems, 1998): the impurities were extracted by DCM from the solution of peptides in 20% acetic acid. The purity and identity of the peptides were determined by the analytical

536 LCMS on an Agilent Technologies 1200 series HPLC connected to an Agilent
537 Technologies 6130 quadrupole LC/MS linked to an Agilent diode array detector.
538
539 *O-(dibenzylphosphono)-N-Fmoc-L-tyrosine*
540 To a solution of Fmoc-tyrosine (2 g, 5 mmol) in anhydrous THF (12 mL) *N*-
541 methylmorpholine (540 µL, 5 mmol) and *tert*-butyldimethylsilyl chloride (740 mg, 4.9 mmol)
542 were added. After 15 min 4,5-dicyanoimidazole (1.8 g, 15 mmol) and
543 diisopropylphosphoramidite (3.4 mL, 10 mmol) were added and the reaction mixture was
544 stirred at room temperature for 4 h. After cooling to 0°C 70% *tert*-butyl hydroperoxide (2
545 ml, 15 mmol) was introduced. After stirring for 2 h at 0°C, 10% $Na_2S_2O_5$ (20 ml) was added
546 and stirring continued for one more hour. The product was extracted with ethyl acetate,
547 washed with a 5% solution of $KHSO_4$, brine, dried over $MgSO_4$, concentrated by rotary
548 evaporation under reduced pressure, and further purified by column chromatography on
549 silica gel using a gradient elution of 0% to 10% of MeOH in DCM to afford *O*-
550 (dibenzylphosphono)-*N*-Fmoc-*L*-tyrosine (3g, 90%) as a pale yellow solid. NMR spectra
551 were in agreement with the published data (Perich and Reynolds, 1991).
552
553 *Isothermal titration calorimetry*
554 Experiments were performed with ITC200 instrument (Malvern) in 100mM HEPES pH7.5,
555 50mM NaCl, 0.5mM TCEP at 298K stirring the sample at 750 rpm. The ITC titration
556 consisted of 0.4 µL initial injection (discarded during data analysis) followed by 19 of 2 µL
557 injections at 120 seconds interval between injections. The GHR_pY595 peptide
558 (PVPDpYTSIHIV-amide, 750 µM) and EpoR_pY426 (ASFEpYTILDPS-amide, 750 µM)
559 were directly titrated into SBC (50 µM). Binding data was subtracted from a control titration
560 where peptide was titrated into buffer, and fitted using a one-set-of-site binding model to
561 obtain dissociation constants, binding enthalpy (ΔH), and stoichiometry (N) using MicroCal
562 ITC-ORIGIN Analysis Software 7.0 (Malven).
563
564 *Surface plasmon resonance*
565 Experiments were performed using Biacore T200 instrument (GH Healthcare) in 20 mM
566 HEPES pH7.5, 150 mM NaCl, 1mM TCEP, 0.005 % Tween20 buffer at 10 °C. Biotinylated
567 wild type SBC and mutants were immobilized onto a chip surface and injected a series of
568 seven concentrations (0.08, 0.25, 0.7, 2.2, 6.7, 20 and 60 µM) of peptide across the
569 sensor surface for 60 sec contact time and 120 sec disassociation time at 30 µl/min flow
570 rate. Data analysis was carried out using Biacore Evaluation Software (GE Healthcare). All

571 data were double-referenced for reference surface and blank injection. The processed
572 sensograms were fit to a steady-state affinity using a 1:1 binding model for K_D estimation.
573
574 *^{19}F ligand NMR*
575 Experiments were conducted using AV-500 NHz Bruker spectrometer equipped with a 5
576 mm CPQCI 1H/19F/13C/15N/D Z-GRD cryoprobe) at 298 K. Spectra were recorded using
577 a Carr-Purcell-Meiboom-Gill (CPMG) pulse sequence that attenuates broad resonances
578 with an interpulse delay at 0.133 seconds for 80 scans. The transmitter frequency was
579 placed close to the resonance of O_1 = -35451 Hz (-75.3 ppm). Protein was used at 5 μM
580 and spy molecule (phosphate **3**) was used at 100 μM in buffer containing 20 mM HEPES
581 pH8, 50 mM NaCl, 1mM DTT, 20 % D_2O. All NMR data were processed and analysed
582 using TopSpin (Bruker).
583
584 Signal contrast between bound and free form of the spy is calculated as below
585

$$Contrast\ (\%) = \frac{Spy_{Free} - Spy_{Bound}}{Spy_{Free}}$$

586
587 where Spy_{free} is the peak integral or T_2 of spy in the absence of protein, while Spy_{bound} is
588 the signal of spy in complex with protein.
589
590 For competition studies, the percentage displacement is calculated as below
591

$$Displacement\ (\%) = \frac{Competitor - Spy_{Bound}}{Spy_{Free} - Spy_{Bound}}$$

592
593 where competitor is the peak integral of spy in the presence of competitor, protein and
594 spy.
595
596 To calculate the dissociation constant of competitor (Ki), assuming all other experimental
597 conditions are identical in the absence and presence of competitor, the signal intensity is
598 proportional to the concentration of protein-spy complex, and can be expressed as below
599 (Wang, Liu and Wyss, 2004)
600

$$\frac{Signal(I)}{Signal(0)} = \frac{[Eo] + [Lo] + K_D - [EI] - \sqrt{([Eo] + [Lo] + K_D - [EI])^2 - 4([Eo] - [EI])[Lo]}}{[Eo] + [Lo] + KD - \sqrt{([Eo] + [Lo] + K_D)^2 - 4[Eo][Lo]}}$$

601

602 where Signal(I) and Signal(0) are the fluorine intensities in the presence and absence of
603 competitor, respectively. [E_0] is the total concentration of protein. [L_0] is the total
604 concentration of ligand. [EL] is concentration of protein-ligand complex. From the observed
605 ratio of signal intensity, the Ki can be calculated.

606

607 **Accession Code**

608 The coordinates and structure factors for SBC in complex with EpoR_pY426 peptide,
609 GHR_pY595 peptide, and GHR2_pY595 peptide have been deposited to the Protein Data
610 Bank (PDB) with accession codes 6I4X, 6I5N, and 6I5J, respectively.

611

612 **Supplemental information**

613 Supplementary Figures S1–S5 are included.

614

615 **Acknowledgements**

616 This project has received funding from the European Research Council (ERC) under the
617 European Union's Seventh Framework Programme (FP7/2007-2013) as a Starting Grant
618 to A.C. (grant agreement No. ERC-2012-StG-311460 DrugE3CRLs). Biophysics and drug
619 discovery activities at Dundee are supported by Wellcome Trust strategic awards
620 (100476/Z/12/Z and 094090/Z/10/Z, respectively). W.K. was supported by a PhD
621 Scholarship by the School of Life Sciences at the University of Dundee. We thank P. Fyfe
622 for support with in-house X-ray facilities, the Diamond Light Source for beamtime (BAG
623 proposals MX14980-13 and MX14980-20) and P. Romano and P. Aller for support at
624 beamlines.

625

626 **Competing interests:** The A.C. laboratory receives sponsored research support from
627 Boehringer Ingelheim and Nurix, Inc. A.C. is a scientific founder, director and shareholder
628 of Amphista Therapeutics, a company that is developing targeted protein degradation
629 therapeutic platforms.

630 **References**

631 Adams, P. D., Afonine, P. V., Bunkóczi, G., Chen, V. B., Davis, I. W., Echols, N., Headd, J.
632 J., Hung, L. W., Kapral, G. J., Grosse-Kunstleve, R. W., McCoy, A. J., Moriarty, N. W.,
633 Oeffner, R., Read, R. J., Richardson, D. C., Richardson, J. S., Terwilliger, T. C. and Zwart,
634 P. H. (2010) 'PHENIX: A comprehensive Python-based system for macromolecular
635 structure solution', *Acta Crystallographica Section D: Biological Crystallography*, 66(2), pp.
636 213–221. doi: 10.1107/S0907444909052925.

637 Alexander, W. S. and Hilton, D. J. (2004) 'The Role of Suppressors of Cytokine Signaling
638 (SOCS) Proteins in Regulation of the Immune Response', *Annual Review of Immunology*,
639 22(1), pp. 503–529. doi: 10.1146/annurev.immunol.22.091003.090312.

640 Armougom, F., Moretti, S., Poirot, O., Audic, S., Dumas, P., Schaeli, B., Keduas, V. and
641 Notredame, C. (2006) 'Expresso: Automatic incorporation of structural information in
642 multiple sequence alignments using 3D-Coffee', *Nucleic Acids Research*. doi:
643 10.1093/nar/gkl092.

644 Babon, J. J., McManus, E. J., Yao, S., DeSouza, D. P., Mielke, L. A., Sprigg, N. S.,
645 Willson, T. A., Hilton, D. J., Nicola, N. A., Baca, M., Nicholson, S. E. and Norton, R. S.
646 (2006) 'The Structure of SOCS3 Reveals the Basis of the Extended SH2 Domain Function
647 and Identifies an Unstructured Insertion That Regulates Stability', *Molecular Cell*, 22(2),
648 pp. 205–216. doi: 10.1016/j.molcel.2006.03.024.

649 Babon, J. J., Sabo, J. K., Zhang, J. G., Nicola, N. A. and Norton, R. S. (2009) 'The SOCS
650 Box Encodes a Hierarchy of Affinities for Cullin5: Implications for Ubiquitin Ligase
651 Formation and Cytokine Signalling Suppression', *Journal of Molecular Biology*, 387(1), pp.
652 162–174. doi: 10.1016/j.jmb.2009.01.024.

653 Bergamin, E., Wu, J. and Hubbard, S. R. (2006) 'Structural Basis for Phosphotyrosine
654 Recognition by Suppressor of Cytokine Signaling-3', *Structure*, 14(8), pp. 1285–1292. doi:
655 10.1016/j.str.2006.06.011.

656 Biosystems, A. (1998) 'Cleavage, Deprotection, and Isolation of Peptides after Fmoc
657 Synthesis', *Technical Bulletin*, (2), pp. 1–12. doi: 10.1038/nrd.2016.29.

658 Bulatov, E. and Ciulli, A. (2015) 'Targeting Cullin–RING E3 ubiquitin ligases for drug
659 discovery: structure, assembly and small-molecule modulation', *Biochemical Journal*,
660 467(3), pp. 365–386. doi: 10.1042/BJ20141450.

661 Bulatov, E., Martin, E. M., Chatterjee, S., Knebel, A., Shimamura, S., Konijnenberg, A.,
662 Johnson, C., Zinn, N., Grandi, P., Sobott, F. and Ciulli, A. (2015) 'Biophysical Studies on
663 Interactions and Assembly of Full-size E3 Ubiquitin Ligase', *Journal of Biological*
664 *Chemistry*, 290(7), pp. 4178–4191. doi: 10.1074/jbc.M114.616664.

665 Bullock, A. N., Debreczeni, J. E., Edwards, A. M., Sundstrom, M. and Knapp, S. (2006)
666 'Crystal structure of the SOCS2-elongin C-elongin B complex defines a prototypical SOCS
667 box ubiquitin ligase', *Proceedings of the National Academy of Sciences*, 103(20), pp.
668 7637–7642. doi: 10.1073/pnas.0601638103.

669 Bullock, A. N., Rodriguez, M. C., Debreczeni, J. É., Songyang, Z. and Knapp, S. (2007)
670 'Structure of the SOCS4-ElonginB/C Complex Reveals a Distinct SOCS Box Interface and
671 the Molecular Basis for SOCS-Dependent EGFR Degradation', *Structure*, 15(11), pp.
672 1493–1504. doi: 10.1016/j.str.2007.09.016.

673 Carr, H. and Purcell, E. (1954) 'Effects of Diffusion on Free Precession in Nuclear
674 Magnetic Resonance Experiments', *Physical Review*, 94(1953), pp. 630–638. doi:
675 10.1103/PhysRev.94.630.

676 Chao, H. G., Leiting, B., Reiss, P. D., Burkhardt, A. L., Klimas, C. E., Bolen, J. B. and
677 Matsueda, G. R. (1995) 'Synthesis and Application of Fmoc-O-
678 [bis(dimethylamino)phosphono]-tyrosine, a Versatile Protected Phosphotyrosine
679 Equivalent', *Journal of Organic Chemistry*. doi: 10.1021/jo00129a001.

680 Dalvit, C., Fagerness, P. E., Hadden, D. T. A., Sarver, R. W. and Stockman, B. J. (2003)
681 'Fluorine-NMR experiments for high-throughput screening: Theoretical aspects, practical
682 considerations, and range of applicability', *Journal of the American Chemical Society*,
683 125(25), pp. 7696–7703. doi: 10.1021/ja034646d.

684 Dey, B. R., Spence, S. L., Nissley, P. and Furlanetto, R. W. (1998) 'Interaction of Human
685 Suppressor of Cytokine Signaling (SOCS)-2 with the Insulin-like Growth Factor-I
686 Receptor', *Journal of Biological Chemistry* , 273(37), pp. 24095–24101. doi:
687 10.1074/jbc.273.37.24095 .

688 Emsley, P., Lohkamp, B., Scott, W. G. and Cowtan, K. (2010) 'Features and development
689 of Coot', *Acta Crystallographica Section D: Biological Crystallography*, 66(4), pp. 486–501.
690 doi: 10.1107/S0907444910007493.

691 Evans, P. R. and Murshudov, G. N. (2013) 'How good are my data and what is the
692 resolution?', *Acta Crystallographica Section D: Biological Crystallography*, 69(7), pp.
693 1204–1214. doi: 10.1107/S0907444913000061.

694 Eyckerman, S., Verhee, A., Van der Heyden, J., Lemmens, I., Van Ostade, X.,
695 Vandekerckhove, J. and Tavernier, J. (2001) 'Design and application of a cytokine-
696 receptor-based interaction trap', *Nature Cell Biology*, 3(12), pp. 1114–1119. doi:
697 10.1038/ncb1201-1114.

698 Farabegoli, F., Ceccarelli, C., Santini, D. and Taffurelli, M. (2005) 'Suppressor of cytokine
699 signalling 2 (SOCS-2) expression in breast carcinoma', *Journal of Clinical Pathology*,
700 58(10), pp. 1046–1050. doi: 10.1136/jcp.2004.024919.

701 Forbes, S. A., Beare, D., Boutselakis, H., Bamford, S., Bindal, N., Tate, J., Cole, C. G.,
702 Ward, S., Dawson, E., Ponting, L., Stefancsik, R., Harsha, B., YinKok, C., Jia, M., Jubb,
703 H., Sondka, Z., Thompson, S., De, T. and Campbell, P. J. (2017) 'COSMIC: Somatic
704 cancer genetics at high-resolution', *Nucleic Acids Research*, 45(D1), pp. D777–D783. doi:
705 10.1093/nar/gkw1121.

706 Gadd, M. S., Bulatov, E. and Ciulli, A. (2015) 'Serendipitous SAD solution for DMSO-
707 Soaked SOCS2-ElonginC-ElonginB crystals using covalently incorporated
708 dimethylarsenic: Insights into substrate receptor conformational flexibility in cullin RING
709 ligases', *PLoS ONE*, 10(6). doi: 10.1371/journal.pone.0131218.

710 Galic, S., Sachithanandan, N., Kay, T. W. and Steinberg, G. R. (2014) 'Suppressor of
711 cytokine signalling (SOCS) proteins as guardians of inflammatory responses critical for
712 regulating insulin sensitivity', *Biochemical Journal*, 461(2), pp. 177–188. doi:
713 10.1042/BJ20140143.

714 Goldschmidt, L., Cooper, D. R., Derewenda, Z. S. and Eisenberg, D. (2007) 'Toward
715 rational protein crystallization: A Web server for the design of crystallizable protein

716 variants', *Protein Science*, 16(8), pp. 1569–1576. doi: 10.1110/ps.072914007.

717 Goldshmit, Y., Walters, C. E., Scott, H. J., Greenhalgh, C. J. and Turnley, A. M. (2004)
718 'SOCS2 induces neurite outgrowth by regulation of epidermal growth factor receptor
719 activation.', *The Journal of biological chemistry*. doi: 10.1074/jbc.M312873200.

720 Greenhalgh, C. J., Bertolino, P., Asa, S. L., Metcalf, D., Corbin, J. E., Adams, T. E., Davey,
721 H. W., Nicola, N. A., Hilton, D. J. and Alexander, W. S. (2002) 'Growth Enhancement in
722 Suppressor of Cytokine Signaling 2 (SOCS-2)-Deficient Mice Is Dependent on Signal
723 Transducer and Activator of Transcription 5b (STAT5b)', *Molecular Endocrinology*, 16(6),
724 pp. 1394–1406. doi: 10.1210/mend.16.6.0845.

725 Greenhalgh, C. J., Metcalf, D., Thaus, A. L., Corbin, J. E., Uren, R., Morgan, P. O., Fabri,
726 L. J., Zhang, J. G., Martin, H. M., Willson, T. A., Billestrup, N., Nicola, N. A., Baca, M.,
727 Alexander, W. S. and Hilton, D. J. (2002) 'Biological evidence that SOCS-2 can act either
728 as an enhancer or suppressor of growth hormone signaling', *Journal of Biological*
729 *Chemistry*, 277(43), pp. 40181–40184. doi: 10.1074/jbc.C200450200.

730 Greenhalgh, C. J., Rico-bautista, E., Lorentzon, M., Thaus, A. L., Morgan, P. O., Willson,
731 T. A., Zervoudakis, P., Metcalf, D., Street, I., Nicola, N. A., Nash, A. D., Fabri, L. J.,
732 Norstedt, G., Ohlsson, C., Flores-morales, A., Alexander, W. S. and Hilton, D. J. (2005)
733 'SOCS2 negatively regulates growth hormone action in vitro and in vivo.', *The Journal of*
734 *clinical investigation*, 115(2), pp. 397–406. doi: 10.1172/JCI22710.

735 Haan, S. (2016) 'SOCS2 physiological and pathological functions', *Frontiers in Bioscience*,
736 8(1), p. 760. doi: 10.2741/760.

737 Haffner, M. C., Petridou, B., Peyrat, J. P., Révillion, F., Müller-Holzner, E., Daxenbichler,
738 G., Marth, C. and Doppler, W. (2007) 'Favorable prognostic value of SOCS2 and IGF-I in
739 breast cancer', *BMC Cancer*, 7. doi: 10.1186/1471-2407-7-136.

740 Hansen, J. a, Lindberg, K., Hilton, D. J., Nielsen, J. H. and Billestrup, N. (1999)
741 'Mechanism of inhibition of growth hormone receptor signaling by suppressor of cytokine
742 signaling proteins.', *Molecular endocrinology (Baltimore, Md.)*, 13(11), pp. 1832–1843. doi:
743 10.1210/mend.13.11.0368.

744 Hoesel, B. and Schmid, J. A. (2013) 'The complexity of NF-κB signaling in inflammation
745 and cancer', *Molecular Cancer*. doi: 10.1186/1476-4598-12-86.

746 Hughes, S. J. and Ciulli, A. (2017) 'Molecular recognition of ternary complexes: a new
747 dimension in the structure-guided design of chemical degraders', *Essays in Biochemistry*,
748 61(October), pp. 505–516. doi: 10.1042/EBC20170041.

749 Inagaki-Ohara, K., Kondo, T., Ito, M. and Yoshimura, A. (2013) 'SOCS, inflammation, and
750 cancer', *JAK-STAT*, 2(3), p. e24053. doi: 10.4161/jkst.24053.

751 Kabsch, W. (2010) 'XDS', *Acta Crystallographica Section D: Biological Crystallography*,
752 66(2), pp. 125–132. doi: 10.1107/S0907444909047337.

753 Kamura, T., Maenaka, K., Kotoshiba, S., Matsumoto, M., Kohda, D., Conaway, R. C.,
754 Conaway, J. W. and Nakayama, K. I. (2004) 'VHL-box and SOCS-box domains determine
755 binding specificity for Cul2-Rbx1 and Cul5-Rbx2 modules of ubiquitin ligases', *Genes and*
756 *Development*, 18(24), pp. 3055–3065. doi: 10.1101/gad.1252404.

757 Kamura, T., Sato, S., Haque, D., Liu, L., Kaelin, W. G., Conaway, R. C. and Conaway, J.
758 W. (1998) 'The Elongin BC complex interacts with the conserved SOCS-box motif present
759 in members of the SOCS, ras, WD-40 repeat, and ankyrin repeat families', *Genes and*
760 *Development*, 12(24), pp. 3872–3881. doi: 10.1101/gad.12.24.3872.

761 Kaneko, T., Huang, H., Zhao, B., Li, L., Liu, H., Voss, C. K., Wu, C., Schiller, M. R. and Li,
762 S. S. C. (2010) 'Loops govern SH2 domain specificity by controlling access to binding
763 pockets', *Science Signaling*, 3(120). doi: 10.1126/scisignal.2000796.

764 Keating, N. and Nicholson, S. E. (2018) 'SOCS-mediated immunomodulation of natural
765 killer cells', *Cytokine*. doi: 10.1016/j.cyto.2018.03.033.

766 Kershaw, N. J., Murphy, J. M., Liau, N. P. D., Varghese, L. N., Laktyushin, A., Whitlock, E.
767 L., Lucet, I. S., Nicola, N. A. and Babon, J. J. (2013) 'SOCS3 binds specific receptor-JAK
768 complexes to control cytokine signaling by direct kinase inhibition', *Nature Structural and*
769 *Molecular Biology*, 20(4), pp. 469–476. doi: 10.1038/nsmb.2519.

770 Kim, Y. K., Kwak, M. J., Ku, B., Suh, H. Y., Joo, K., Lee, J., Jung, J. U. and Oh, B. H.
771 (2013) 'Structural basis of intersubunit recognition in elongin BC-cullin 5-SOCS box
772 ubiquitin-protein ligase complexes', *Acta Crystallographica Section D: Biological*
773 *Crystallography*, 69(8), pp. 1587–1597. doi: 10.1107/S0907444913011220.

774 Lavens, D. (2006) 'A complex interaction pattern of CIS and SOCS2 with the leptin
775 receptor', *Journal of Cell Science*, 119(11), pp. 2214–2224. doi: 10.1242/jcs.02947.

776 Liau, N. P. D., Laktyushin, A., Lucet, I. S., Murphy, J. M., Yao, S., Whitlock, E., Callaghan,
777 K., Nicola, N. A., Kershaw, N. J. and Babon, J. J. (2018) 'The molecular basis of
778 JAK/STAT inhibition by SOCS1', *Nature Communications*. doi: 10.1038/s41467-018-
779 04013-1.

780 Linossi, E. M., Babon, J. J., Hilton, D. J. and Nicholson, S. E. (2013) 'Suppression of
781 cytokine signaling: The SOCS perspective', *Cytokine and Growth Factor Reviews*, pp.
782 241–248. doi: 10.1016/j.cytogfr.2013.03.005.

783 Linossi, E. M. and Nicholson, S. E. (2012) 'The SOCS box-adapting proteins for
784 ubiquitination and proteasomal degradation.', *IUBMB life*, 64(4), pp. 316–23. doi:
785 10.1002/iub.1011.

786 Liu, C., Li, Y., Semenov, M., Han, C., Baeg, G. H., Tan, Y., Zhang, Z., Lin, X. and He, X.
787 (2002) 'Control of β-catenin phosphorylation/degradation by a dual-kinase mechanism',
788 *Cell*. doi: 10.1016/S0092-8674(02)00685-2.

789 Liu, J. and Nussinov, R. (2009) 'The mechanism of ubiquitination in the cullin-RING E3
790 ligase machinery: Conformational control of substrate orientation', *PLoS Computational*
791 *Biology*, 5(10). doi: 10.1371/journal.pcbi.1000527.

792 Lu, J., Qian, Y., Altieri, M., Dong, H., Wang, J., Raina, K., Hines, J., Winkler, J. D., Crew,
793 A. P., Coleman, K. and Crews, C. M. (2015) 'Hijacking the E3 Ubiquitin Ligase Cereblon to
794 Efficiently Target BRD4', *Chemistry & biology*. 2015/06/04, 22(6), pp. 755–763. doi:
795 10.1016/j.chembiol.2015.05.009.

796 Lucas, X. and Ciulli, A. (2017) 'Recognition of substrate degrons by E3 ubiquitin ligases
797 and modulation by small-molecule mimicry strategies', *Current Opinion in Structural*
798 *Biology*, pp. 101–110. doi: 10.1016/j.sbi.2016.12.015.

799 Maniaci, C., Hughes, S. J., Testa, A., Chen, W., Lamont, D. J., Rocha, S., Alessi, D. R.,
800 Romeo, R. and Ciulli, A. (2017) 'Homo-PROTACs: bivalent small-molecule dimerizers of
801 the VHL E3 ubiquitin ligase to induce self-degradation', *Nature Communications*, 8(1), p.
802 830. doi: 10.1038/s41467-017-00954-1.

803 McCoy, A. J., Grosse-Kunstleve, R. W., Adams, P. D., Winn, M. D., Storoni, L. C. and
804 Read, R. J. (2007) 'Phaser crystallographic software', *Journal of Applied Crystallography*,
805 40(4), pp. 658–674. doi: 10.1107/S0021889807021206.

806 McCoy, A. J., Storoni, L. C. and Read, R. J. (2004) 'Simple algorithm for a maximum-
807 likelihood SAD function', *Acta Crystallographica Section D: Biological Crystallography*,
808 60(7), pp. 1220–1228. doi: 10.1107/S0907444904009990.

809 Meiboom, S., Gill, D. and Gillt, D. (1958) 'Modified Spin-Echo Method for Measuring
810 Nuclear Relaxation Times Modified Spin-Echo Method for Measuring Nuclear Relaxation
811 Times*', *Citation: Review of Scientific Instruments J. Chem. Phys. J. Appl. Phys. J. Chem.*
812 *Phys. J. Appl. Phys. Spin-Echo Method for Measuring Relaxation Times in Two-Line NMR*
813 *Spectra Rev. Sci. Instrum*, 29(8), pp. 214504–2174. doi: 10.1063/1.334358.

814 Mészáros, B., Kumar, M., Gibson, T. J., Uyar, B. and Dosztányi, Z. (2017) 'Degrons in
815 cancer', *Science Signaling*. doi: 10.1126/scisignal.aak9982.

816 Metcalf, D., Greenhalgh, C. J., Viney, E., Wilison, T. A., Starr, R., Nicola, N. A., Hilton, D.
817 J. and Alexander, W. S. (2000) 'Gigantism in mice lacking suppressor of cytokine
818 signalling-2', *Nature*, 405(6790), pp. 1069–1073. doi: 10.1038/35016611.

819 Murshudov, G. N., Skubák, P., Lebedev, A. A., Pannu, N. S., Steiner, R. A., Nicholls, R.
820 A., Winn, M. D., Long, F. and Vagin, A. A. (2011) 'REFMAC5 for the refinement of
821 macromolecular crystal structures', *Acta Crystallographica Section D: Biological*
822 *Crystallography*, 67(4), pp. 355–367. doi: 10.1107/S0907444911001314.

823 Oeckinghaus, A. and Ghosh, S. (2009) 'The NF-kappaB family of transcription factors and
824 its regulation.', *Cold Spring Harbor perspectives in biology*. doi:
825 10.1101/cshperspect.a000034.

826 Ottis, P. and Crews, C. M. (2017) 'Proteolysis-Targeting Chimeras: Induced Protein
827 Degradation as a Therapeutic Strategy', *ACS Chemical Biology*. American Chemical
828 Society, 12(4), pp. 892–898. doi: 10.1021/acschembio.6b01068.

829 Paul, I., Batth, T. S., Iglesias-Gato, D., Al-Araimi, A., Al-Haddabi, I., Alkharusi, A.,
830 Norstedt, G., Olsen, J. V., Zadjali, F. and Flores-Morales, A. (2017) 'The ubiquitin ligase
831 Cullin5 SOCS2 regulates NDR1/STK38 stability and NF-κB transactivation', *Scientific*
832 *Reports*, 7. doi: 10.1038/srep42800.

833 Perich, J. W. and Reynolds, E. C. (1991) 'The Facile One-Pot Synthesis of Nα-(9-
834 Fluorenylmethoxycarbonyl)-O-(O′, O″-dialkylphosphoro)-L-tyrosines Using Dialkyl N,N-
835 Diethylphosphoramidites', *Synlett*, 1991(08), pp. 577–578. doi: 10.1055/s-1991-20804.

836 Piessevaux, J., De Ceuninck, L., Catteeuw, D., Peelman, F. and Tavernier, J. (2008)
837 'Elongin B/C recruitment regulates substrate binding by CIS', *Journal of Biological*
838 *Chemistry*. doi: 10.1074/jbc.M803742200.

839 Piessevaux, J., Lavens, D., Montoye, T., Wauman, J., Catteeuw, D., Vandekerckhove, J.,
840 Belsham, D., Peelman, F. and Tavernier, J. (2006) 'Functional cross-modulation between

841 SOCS proteins can stimulate cytokine signaling', *Journal of Biological Chemistry*, 281(44),
842 pp. 32953–32966. doi: 10.1074/jbc.M600776200.

843 Piessevaux, J., Lavens, D., Peelman, F. and Tavernier, J. (2008) 'The many faces of the
844 SOCS box', *Cytokine and Growth Factor Reviews*. doi: 10.1016/j.cytogfr.2008.08.006.

845 Qiu, X., Zheng, J., Guo, X., Gao, X., Liu, H., Tu, Y. and Zhang, Y. (2013) 'Reduced
846 expression of SOCS2 and SOCS6 in hepatocellular carcinoma correlates with aggressive
847 tumor progression and poor prognosis', *Molecular and Cellular Biochemistry*, 378(1–2),
848 pp. 99–106. doi: 10.1007/s11010-013-1599-5.

849 Ram, P. A. and Waxman, D. J. (1999) 'SOCS/CIS protein inhibition of growth hormone-
850 stimulated STAT5 signaling by multiple mechanisms', *Journal of Biological Chemistry*,
851 274(50), pp. 35553–35561. doi: 10.1074/jbc.274.50.35553.

852 Rico-Bautista, E., Flores-Morales, A. and Fernández-Pérez, L. (2006) 'Suppressor of
853 cytokine signaling (SOCS) 2, a protein with multiple functions.', *Cytokine & growth factor*
854 *reviews*. doi: 10.1016/j.cytogfr.2006.09.008.

855 Sasaki, A., Yasukawa, H., Suzuki, A., Kamizono, S., Syoda, T., Kinjyo, I., Sasaki, M.,
856 Johnston, J. A. and Yoshimura, A. (1999) 'Cytokine-inducible SH2 protein-3
857 (CIS3/SOCS3) inhibits Janus tyrosine kinase by binding through the N-terminal kinase
858 inhibitory region as well as SH2 domain', *Genes to Cells*, 4(6), pp. 339–351. doi:
859 10.1046/j.1365-2443.1999.00263.x.

860 Sato, N. and Miyajima, A. (1994) 'Multimeric cytokine receptors: common versus specific
861 functions', *Current Opinion in Cell Biology*, 6(2), pp. 174–179. doi: 10.1016/0955-
862 0674(94)90133-3.

863 Starr, R., Willson, T. A., Viney, E. M., Murray, L. J. L., Rayner, J. R., Jenkins, B. J., Gonda,
864 T. J., Alexander, W. S., Metcalf, D., Nicola, N. A. and Hilton, D. J. (1997) 'A family of
865 cytokine-inducible inhibitors of signalling', *Nature*, 387(6636), pp. 917–921. doi:
866 10.1038/43206.

867 Stofega, M. R., Herrington, J., Billestrup, N. and Carter-Su, C. (2000) 'Mutation of the
868 SHP-2 binding site in growth hormone (GH) receptor prolongs GH-promoted tyrosyl
869 phosphorylation of GH receptor, JAK2, and STAT5B.', *Molecular endocrinology*
870 *(Baltimore, Md.)*, 14(September), pp. 1338–1350. doi: 10.1210/me.14.9.1338.

871 Sutherland, K. D., Lindeman, G. J., Choong, D. Y. H., Wittlin, S., Brentzell, L., Phillips, W.,
872 Campbell, I. G. and Visvader, J. E. (2004) 'Differential hypermethylation of SOCS genes in
873 ovarian and breast carcinomas', *Oncogene*, 23(46), pp. 7726–7733. doi:
874 10.1038/sj.onc.1207787.

875 Tannahill, G. M., Elliott, J., Barry, A. C., Hibbert, L., Cacalano, N. A. and Johnston, J. A.
876 (2005) 'SOCS2 Can Enhance Interleukin-2 (IL-2) and IL-3 Signaling by Accelerating
877 SOCS3 Degradation', *Molecular and Cellular Biology*, 25(20), pp. 9115–9126. doi:
878 10.1128/MCB.25.20.9115-9126.2005.

879 Terwilliger, T. C., Grosse-Kunstleve, R. W., Afonine, P. V., Moriarty, N. W., Zwart, P. H.,
880 Hung, L. W., Read, R. J. and Adams, P. D. (2007) 'Iterative model building, structure
881 refinement and density modification with the PHENIX AutoBuild wizard', in *Acta*
882 *Crystallographica Section D: Biological Crystallography*, pp. 61–69. doi:
883 10.1107/S090744490705024X.

Turnley, A. M. (2005) ‘Role of SOCS2 in growth hormone actions’, *Trends in Endocrinology and Metabolism*. doi: 10.1016/j.tem.2005.01.006.

Vesterlund, M., Zadjali, F., Persson, T., Nielsen, M. L., Kessler, B. M., Norstedt, G. and Flores-Morales, A. (2011) ‘The SOCS2 ubiquitin ligase complex regulates growth hormone receptor levels’, *PLoS ONE*, 6(9). doi: 10.1371/journal.pone.0025358.

Wang, Y. Sen, Liu, D. and Wyss, D. F. (2004) ‘Competition STD NMR for the detection of high-affinity ligands and NMR-based screening’, *Magnetic Resonance in Chemistry*, 42(6), pp. 485–489. doi: 10.1002/mrc.1381.

Wikman, H., Kettunen, E., Seppänen, J. K., Karjalainen, A., Hollmén, J., Anttila, S. and Knuutila, S. (2002) ‘Identification of differentially expressed genes in pulmonary adenocarcinoma by using cDNA array’, *Oncogene*, 21(37), pp. 5804–5813. doi: 10.1038/sj.onc.1205726.

Winn, M. D., Ballard, C. C., Cowtan, K. D., Dodson, E. J., Emsley, P., Evans, P. R., Keegan, R. M., Krissinel, E. B., Leslie, A. G. W., McCoy, A., McNicholas, S. J., Murshudov, G. N., Pannu, N. S., Potterton, E. A., Powell, H. R., Read, R. J., Vagin, A. and Wilson, K. S. (2011) ‘Overview of the CCP4 suite and current developments’, *Acta Crystallographica Section D: Biological Crystallography*, pp. 235–242. doi: 10.1107/S0907444910045749.

Winter, G. E., Buckley, D. L., Paulk, J., Roberts, J. M., Souza, A., Dhe-Paganon, S. and Bradner, J. E. (2015) ‘Phthalimide conjugation as a strategy for in vivo target protein degradation’, *Science*, 348(6241), p. 1376 LP-1381. Available at: http://science.sciencemag.org/content/348/6241/1376.abstract.

Yang, X. O., Zhang, H., Kim, B. S., Niu, X., Peng, J., Chen, Y., Kerketta, R., Lee, Y. H., Chang, S. H., Corry, D. B., Wang, D., Watowich, S. S. and Dong, C. (2013) ‘The signaling suppressor CIS controls proallergic T cell development and allergic airway inflammation’, *Nature Immunology*, 14(7), pp. 732–740. doi: 10.1038/ni.2633.

Yasukawa, H. (1999) ‘The JAK-binding protein JAB inhibits Janus tyrosine kinase activity through binding in the activation loop’, *The EMBO Journal*, 18(5), pp. 1309–1320. doi: 10.1093/emboj/18.5.1309.

Yoshimura, a, Ohkubo, T., Kiguchi, T., Jenkins, N. a, Gilbert, D. J., Copeland, N. G., Hara, T. and Miyajima, a (1995) ‘A novel cytokine-inducible gene CIS encodes an SH2-containing protein that binds to tyrosine-phosphorylated interleukin 3 and erythropoietin receptors.’, *The EMBO journal*, 14(12), pp. 2816–2826. doi: 10.1182/BLOOD.V97.8.2230.

Yoshimura, A., Naka, T. and Kubo, M. (2007) ‘SOCS proteins, cytokine signalling and immune regulation’, *Nature Reviews Immunology*, pp. 454–465. doi: 10.1038/nri2093.

Zadjali, F., Pike, A. C. W., Vesterlund, M., Sun, J., Wu, C., Li, S. S. C., Rönnstrand, L., Knapp, S., Bullock, A. N. and Flores-Morales, A. (2011) ‘Structural basis for c-KIT inhibition by the suppressor of cytokine signaling 6 (SOCS6) ubiquitin ligase’, *Journal of Biological Chemistry*, 286(1), pp. 480–490. doi: 10.1074/jbc.M110.173526.

Zengerle, M., Chan, K. H. and Ciulli, A. (2015) ‘Selective Small Molecule Induced Degradation of the BET Bromodomain Protein BRD4’, *ACS Chemical Biology*, 10(8), pp. 1770–1777. doi: 10.1021/acschembio.5b00216.

Zhang, J. G., Farley, a, Nicholson, S. E., Willson, T. a, Zugaro, L. M., Simpson, R. J., Moritz, R. L., Cary, D., Richardson, R., Hausmann, G., Kile, B. J., Kent, S. B., Alexander, W. S., Metcalf, D., Hilton, D. J., Nicola, N. a and Baca, M. (1999) 'The conserved SOCS box motif in suppressors of cytokine signaling binds to elongins B and C and may couple bound proteins to proteasomal degradation.', *Proceedings of the National Academy of Sciences of the United States of America*, 96(5), pp. 2071–2076. doi: 10.1073/pnas.96.5.2071.

Zhang, Y., Zhang, J., Yuan, C., Hard, R. L., Park, I. H., Li, C., Bell, C. and Pei, D. (2011) 'Simultaneous binding of two peptidyl ligands by a Src homology 2 domain', *Biochemistry*, 50(35), pp. 7637–7646. doi: 10.1021/bi200439v.

Zhu, J. G., Dai, Q. S., Han, Z. D., He, H. C., Mo, R. J., Chen, G., Chen, Y. F., Wu, Y. D., Yang, S. B., Jiang, F. N., Chen, W. H., Sun, Z. L. and Zhong, W. De (2013) 'Expression of SOCSs in human prostate cancer and their association in prognosis', *Molecular and Cellular Biochemistry*, 381(1–2), pp. 51–59. doi: 10.1007/s11010-013-1687-6.

942 **Figures and Schemes**

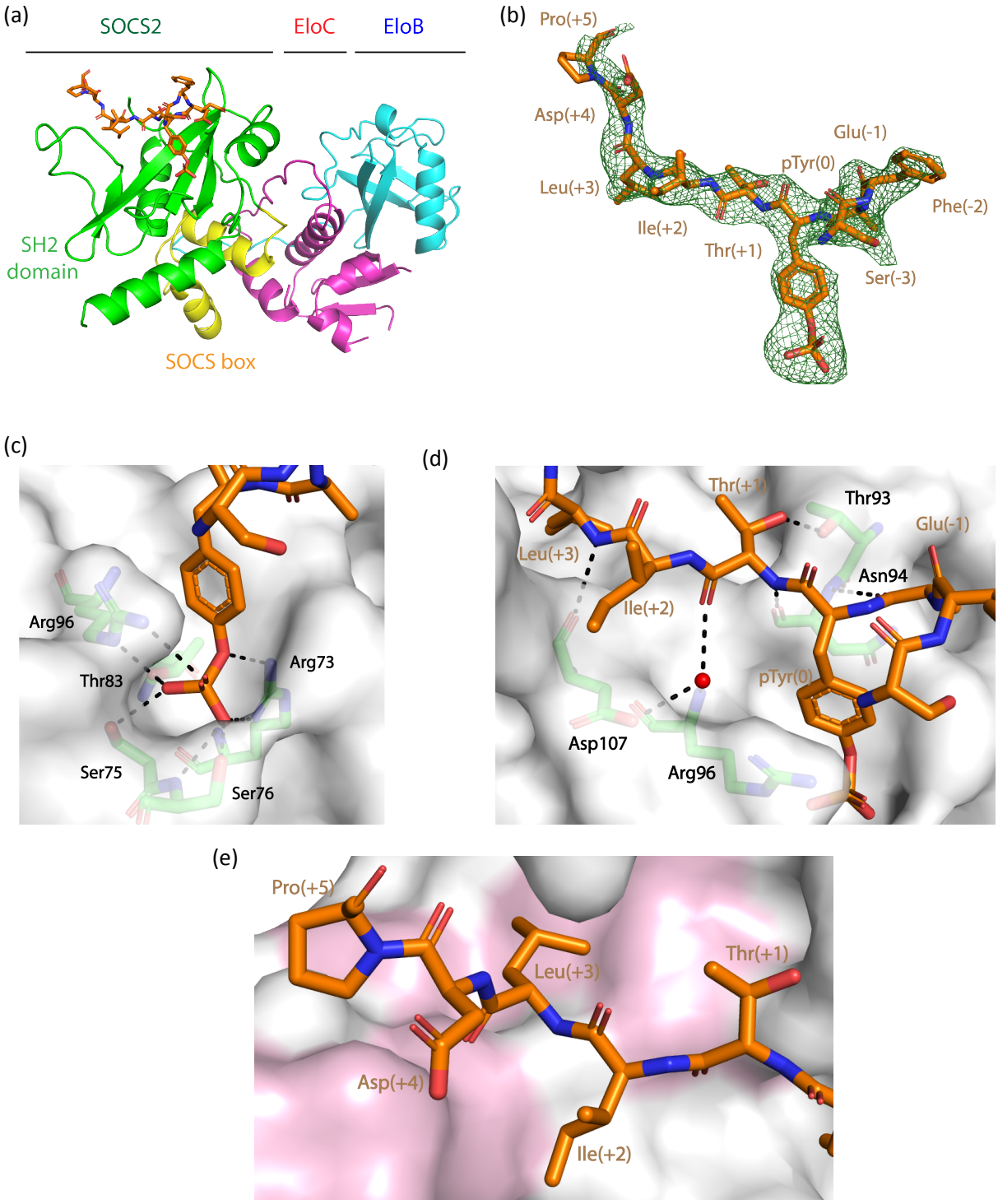

943

944 **Figure 1. Structural and interaction detail of the SBC-EpoR co-crystal**

945 (a) Domain and protein arrangement of the SBC-EpoR co-crystal. Protein chains are shown in
946 cartoon, with EloB (cyan), EloC (magenta) and SOCS2, comprising of SOCS box (yellow) and SH2
947 domain (green). The EpoR_pY426 peptide is shown in orange stick. (b) The Fo-Fc ligand omit map
948 of the EpoR_pY426 peptide (green mesh) contoured at 2.0 σ level to highlight densities for the
949 EpoR_pY426 peptide (orange stick) (c) Hydrogen bond interactions (dash) between the pY of
950 EpoR_pY426 peptide (orange stick) and SOCS2 (green). (d) Hydrogen bond interaction (dash)
951 between the EpoR_pY426 peptide (orange stick), SOCS2 (green stick) and water (red sphere). (e)
952 Hydrophobic interaction between EpoR_pY426 peptide (orange stick) and SOCS2 (surface).
953 Hydrophobic residues on SOCS2 are colored in pink.

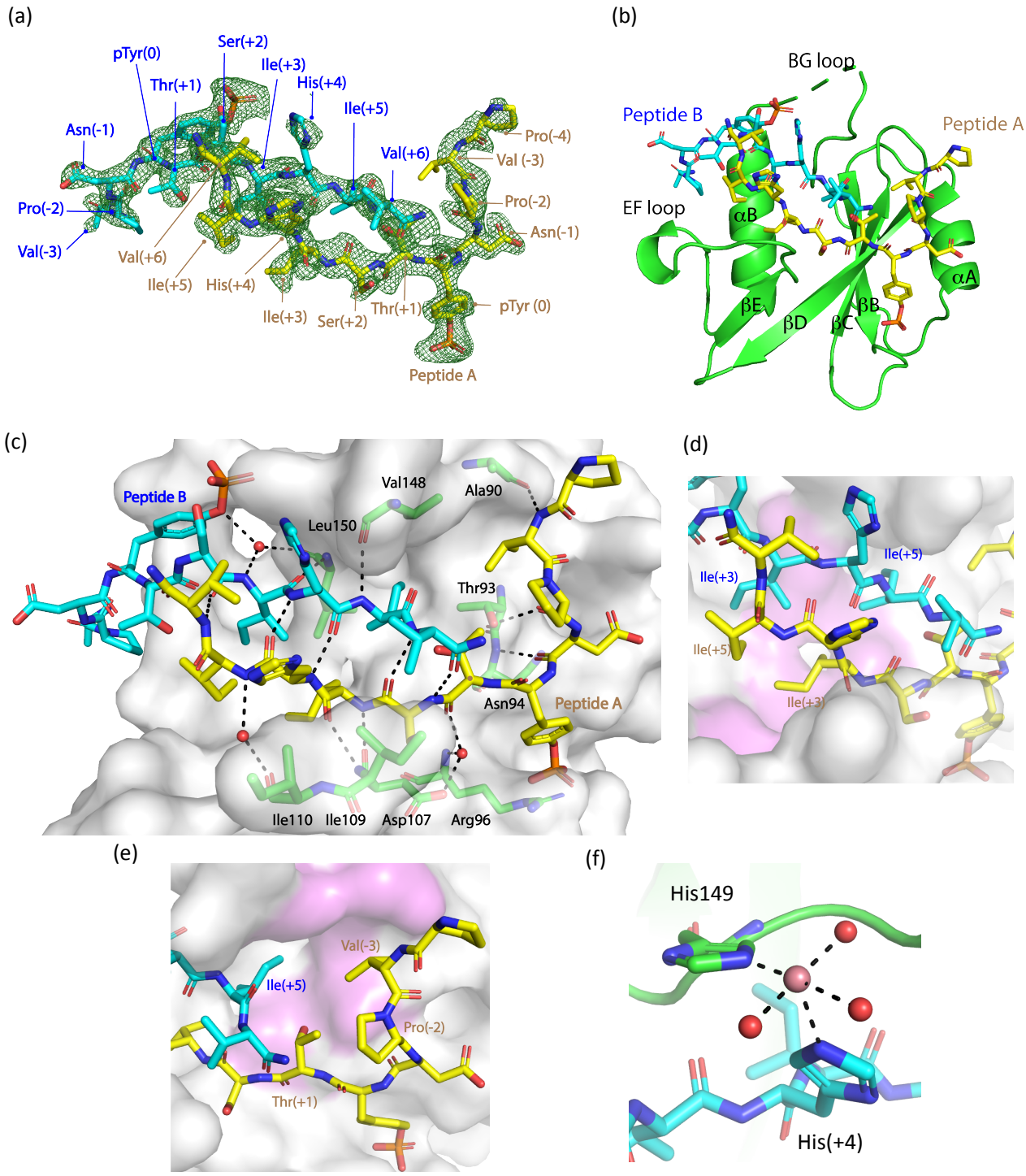

954

955 **Figure 2. Structural and interaction detail of the SBC-GHR co-crystal**

956 Two copies of GHR_pY595 were observed in the co-crystal. One copy is shown as peptide
957 A (yellow stick) and the other one as peptide B (cyan stick). (a) The Fo-Fc ligand omit map
958 of the peptides (green mesh) contoured at 2.5 σ level to highlight densities for the peptide
959 A and peptide B (yellow and cyan stick). (b) Cartoon diagram of the SH2 domain of
960 SOCS2 (green) with peptides A and peptide B. (c) Hydrogen bond interactions (dash)
961 among peptide A, peptide B, SOCS2 (green stick) and water (red sphere). (d) (d)(e)
962 Hydrophobic interaction of the peptides with C-terminal half and N-terminal half of the SH2
963 domain (surface), respectively. SOCS2 residues involved in hydrophobic interactions are
964 coloured in pink. (f) The coordination of cobalt ion (pink sphere) with His149 of SOCS2
965 (green), His(+4) of peptide B and water molecules (red sphere).

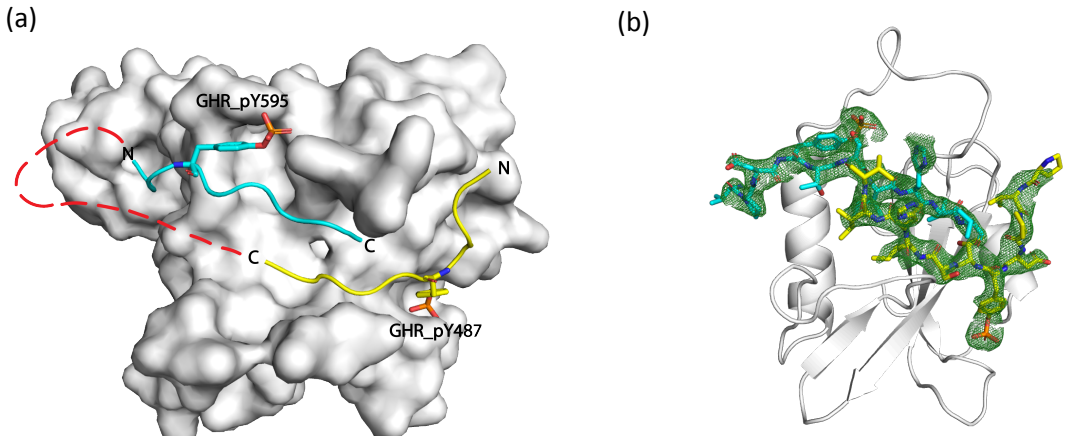

Figure 3. GHR dual-peptide binding mode

(a) Illustration of the hypothesis where the two binding sites on GHR, pY487 and pY595, folded into a hairpin structure for SOCS2 binding. SOCS2 is shown in white surface, the hairpin structure is illustrated by connecting the two peptides (yellow and cyan cartoon) with red dash lines. (b). The Fo-Fc ligand omit map of the GHR peptides (green mesh) contoured at 2.5 σ level to highlight densities for the GHR_pY595 peptides (yellow and cyan stick).

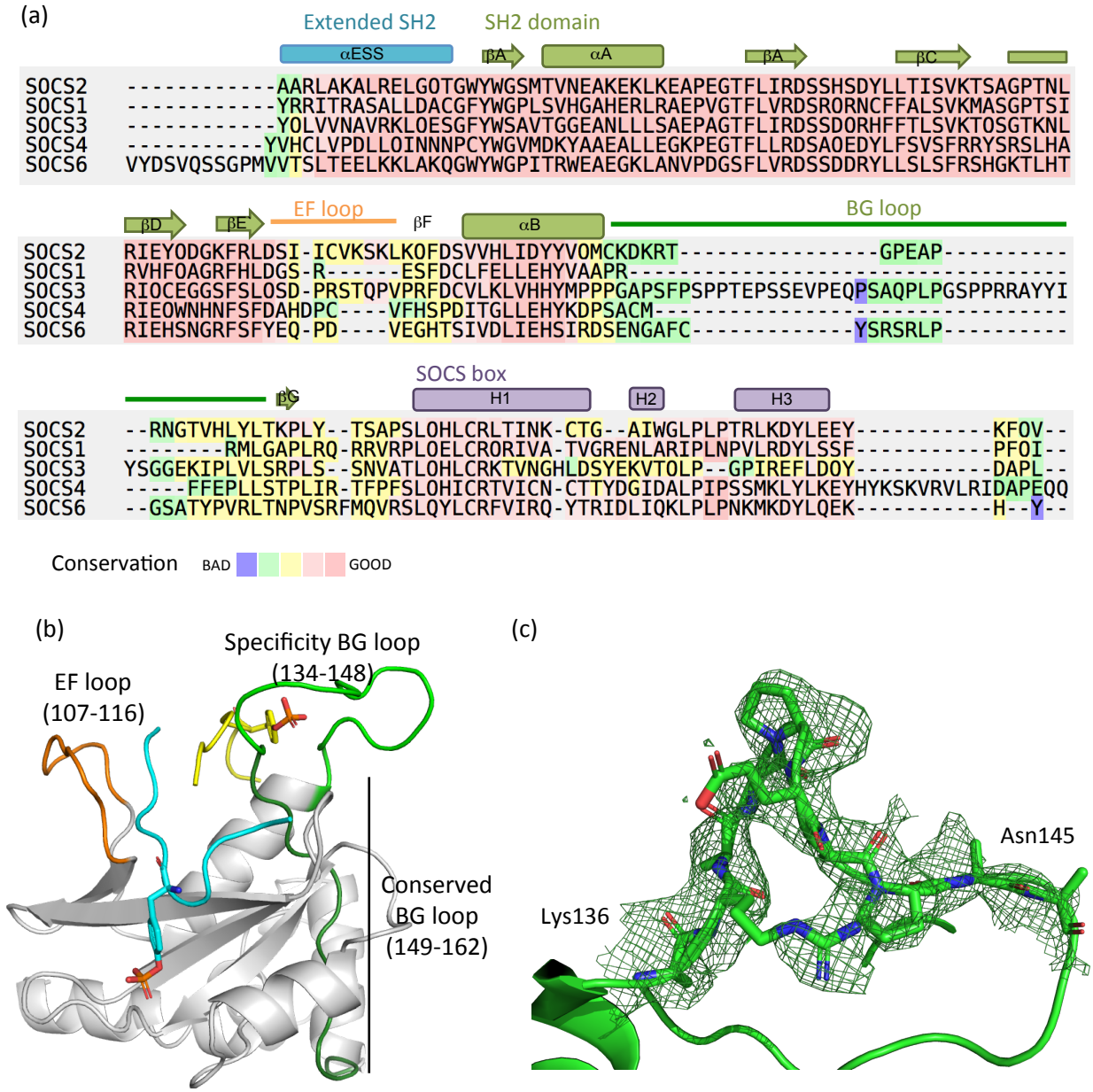

Figure 4. The BG loop of SOCS2

(a) Secondary structure elements in SOCS2 are shown above the sequence alignment. SOCS proteins with structure available were aligned using T-Coffee expresso mode for sequence alignment with structural information (Armougom *et al.*, 2006). (b) Locations of the EF loop (orange) and the BG loop (green) on SOCS2 (white). (c) The Fo-Fc ligand omit map of the previously disordered BG loop (green mesh) contoured at 1.5 σ level.

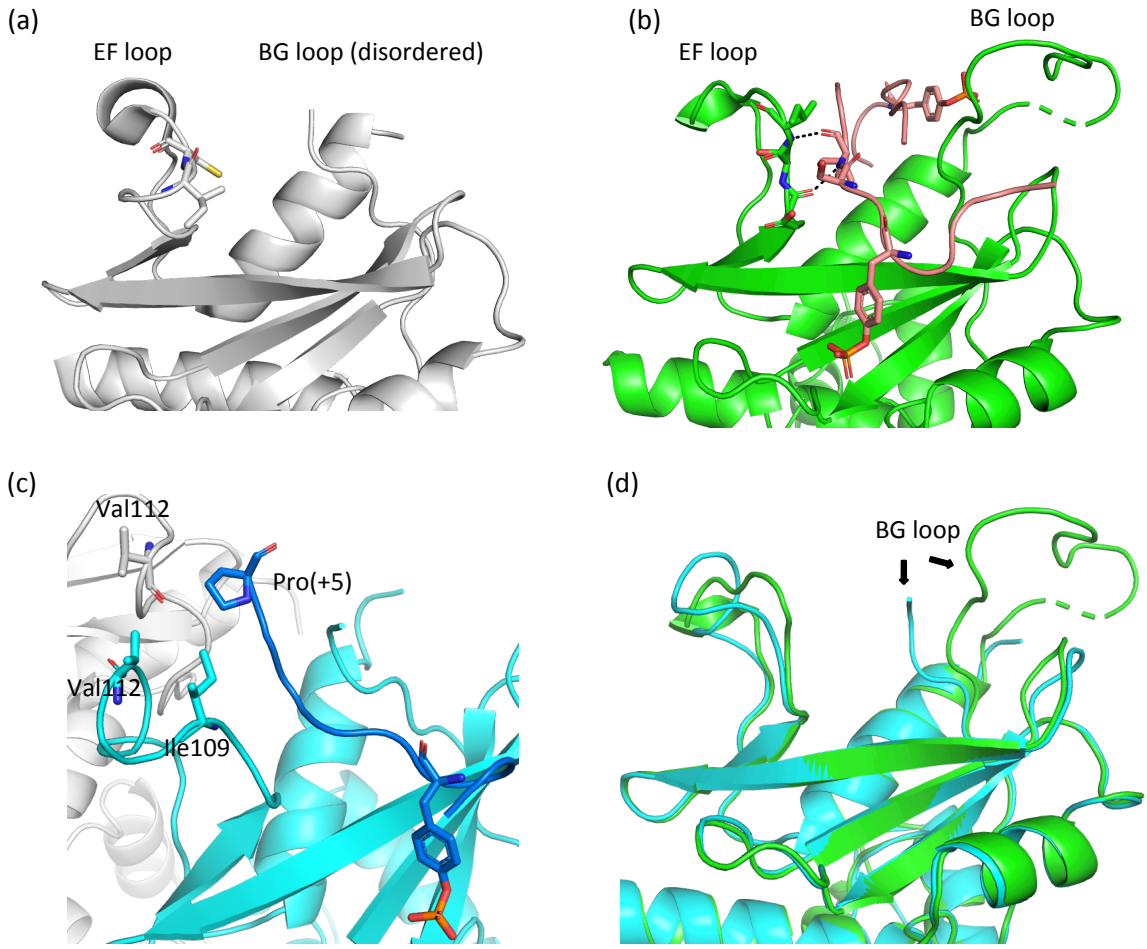

983

984 **Figure 5. Conformation changes of the EF and BG loops**

985 (a) The EF loop curls up in the apo SOCS2 (white, PDB code: 2C9W), placing Ile110 and
986 Cys111 (stick) at the SH2 hydrophobic pocket. (b) The EF loop makes backbone
987 interactions with GHR peptide (pink) in the SBC-GHR_2 structure. (c) The Ile109 and Val
988 112 of SCOS2 (cyan) and Val112 of SOCS2 symmetry mate (white) make unique
989 hydrophobic interaction with Pro(+5) of EpoR peptide (blue). (d) Superposition of the
990 SOCS2 from SBC-GHR_2 (green) and SBC-EpoR (cyan) displays conformational changes
991 of the BG loop.
992

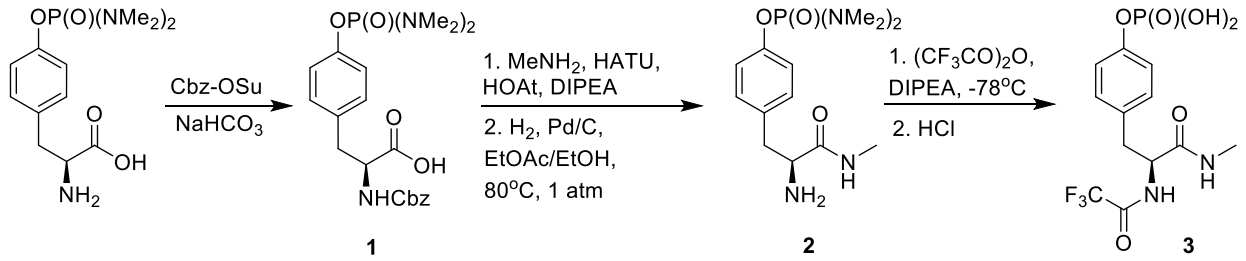

Scheme 1. Synthesis of spy molecule 3

(a)

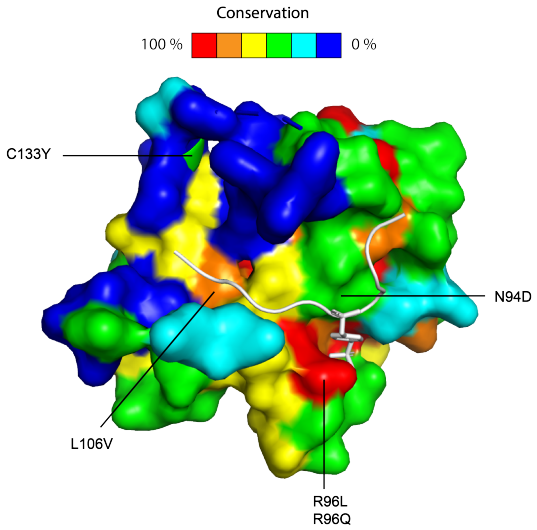

(b)

Protein	SPR K_D (μM) ± SE		
	GHR_pY595	GHR_pY487	EpoR_pY426
Wild type	2.1 ± 0.37	2.8 ± 0.33	10.8 ± 0.64
L106V	2.7 ± 0.36	6.8 ± 1.2	10.4 ± 1.9
C133Y	2.5 ± 0.42	5.6 ± 1.0	11 ± 1.9
N94D	n.b.	weak	n.b.
R96L	weak	weak	n.b.
R96Q	n.b.	n.b.	n.b.

The K_D measurement by SPR was performed with a single experiment, the SE denotes uncertainties of fit to the calculated K_D
weak = saturation was not achieved
n.b. = no binding

(c)

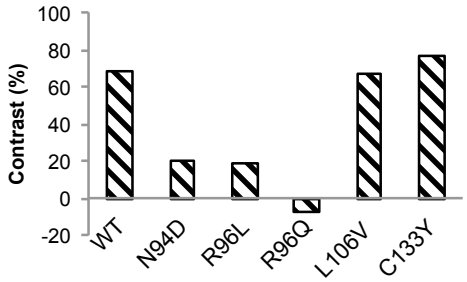

Figure 6. Characterization of SNP containing SOCS2 by SPR and ^{19}F-NMR

(a) Sequence conservation mapped onto the SH2 domain of SOCS2 surface. Conservation surface representation based upon the ClustalW multiple sequence alignment of CIS and SOCS1 – SOCS7 sequences where highly conserved residues are shown in red/orange colour and variable residue positions coloured blue. (b) K_D estimation of peptide binding against SBC proteins from SPR data. (c) Signal contrast of the spy molecule in the absence and presence of SBC proteins.

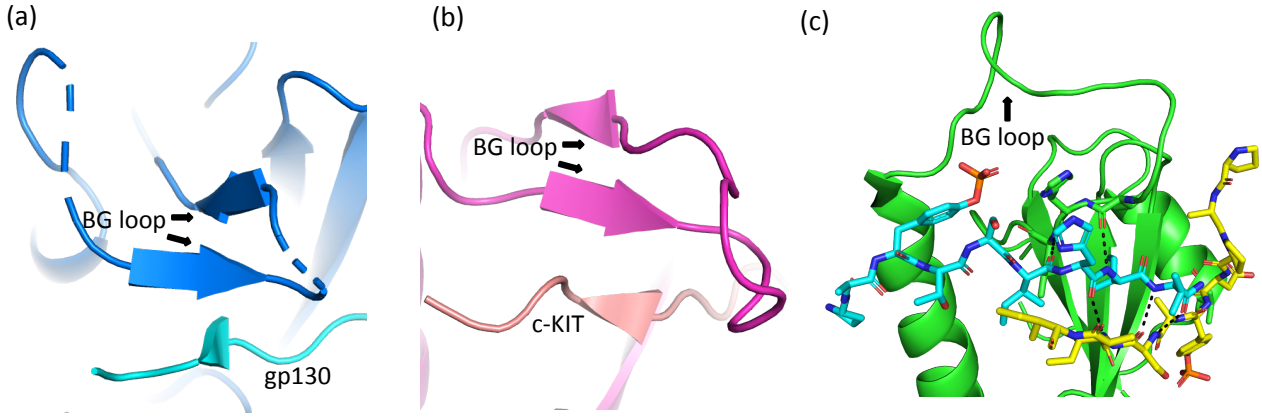

Figure 7. The triple-stranded b-sheet interaction between substrate peptide and protein

(a) The SOCS3 (blue) in complex with gp130 (cyan) (PDB code: 2HMH) (B) The SOCS6 (magenta) in complex with c-Kit (pink) (PBD code: 2VIF) (C) The SOCS2 (green) in complex with GHR_pY595 peptides. Peptide A is shown in yellow stick and peptide B in cyan stick.

1013 **Tables**

1014 **Table 1. Data collection and refinement statistics**

	SBC-EpoR	SBC-GHR	SBC-GHR$_2$
PDB code	6I4X	6I5N	6I5J
Data collection			
Wavelength (Å)	0.9686	0.9795	0.9686
Space group	I 1 2 1	P 2_1 2_1 2	P 2 2_1 2_1
Cell dimensions			
a, b, c (Å)	41.29, 56.33, 203.39	113.55, 157.84, 57.72	57.83, 113.71, 156.94
α, β, γ (°)	90.00, 91.53, 90.00	90.00, 90.00, 90.00	90.00, 90.00, 90.00
Molecules/ASU	1	2	2
Resolution	29.36–2.69 (2.82–2.69)	113.55–1.98 (2.01–1.98)	92.08–2.80 (2.95–2.80)
R_{merge} (%)	10.8 (51.4)	9.4 (103.5)	19 (72.1)
$\langle I/\sigma (I)\rangle$	9.6 (2.4)	17.1 (2.2)	7.3 (2.7)
Completeness (%)	93.2 (63.3)	100 (100)	100 (100)
Redundancy	4.9 (4.2)	13.3 (13.2)	7.8 (7.8)
$CC_{1/2}$	0.99 (0.82)	1.0 (0.9)	0.98 (0.74)
Refinement			
Resolution (Å)	2.69	1.97	2.8
Unique reflections	12273 (1104)	73249(6735)	26321(3761)
R_{work}/R_{free} (%)	19.64/23.51	19.26/23.31	20.96/26.38
Wilson B factor (Å^2)	44.1	24.2	42.5
Average B factor (Å^2)	46.9	32.1	42.5
No. non-hydrogen atoms Protein/ligand/water	2688/83/11	6432/86/516	5775/327/33
R.M.S.D.			
Bond lengths (Å)	0.002	0.015	0.002
Bond angles (°)	0.451	1.29	0.412
Ramachandran analysis			
Preferred regions (%)	96.12	97.51	96.83
Allowed regions (%)	3.58	2.49	3.17
Outliers (%)	0.3	0.00	0.00

1015 Values in parentheses are for the highest resolution shell
1016

1017

1018 **Table 2. Binding affinities of the GHR peptide and Val(-3) analogues**

1019

Protein	sequence	K_D by SPR (μM)	K_D by NMR (μM)
Wild type	PVPDYTSIHIV	1.3 ± 0.14	1.3
V(-3)R	P**R**PDYTSIHIV	9.5 ± 0.43	12.1
V(-3)Y	P**Y**PDYTSIHIV	3.4 ± 0.37	3.4

1020 Residue mutated in bold

1021 The K_D measurement by SPR was performed with a single experiment, the SE denotes
1022 uncertainties of fit to the calculated K_D

1023 The NMR was performed with a single experiment at a fixed CPMG delay, therefore no standard
1024 error can be estimated.
1025

1026 **Table 3. K_D measurement for the GHR_pY595 and EpoR_pY426 derivatives by SPR**
1027 **and ^{19}F NMR**

1028

Sequence	Ala. position	SPR K_D ± SE (μM)	NMR K_D (μM)
PVPDpYTSIHIV	GHR wild type	1.3 ± 0.14	1.3
AVPDpYTSIHIV	pY(-4)	2.1 ± 0.32	1.2
P**A**PDpYTSIHIV	pY(-3)	3.2 ± 0.31	3.6
PV**A**DpYTSIHIV	pY(-2)	1.7 ± 0.22	2.1
PVP**A**pYTSIHIV	pY(-1)	5.8 ± 0.48	11.0
PVPDpY**A**SIHIV	pY(+1)	0.9 ± 0.20	0.6
PVPDpYT**A**IHIV	pY(+2)	1.3 ± 0.23	1.1
PVPDpYTS**A**HIV	pY(+3)	4.2 ± 0.38	4.4
PVPDpYTSI**A**IV	pY(+4)	4.4 ± 0.24	17.3
PVPDpYTSIH**A**V	pY(+5)	2.3 ± 0.31	2.1
PVPDpYTSIHI**A**	pY(+6)	2.0 ± 0.28	1.8
ASFEpYTILDPS	EpoR wild type	12.1 ± 0.92	8.6
A**A**FEpYTILDPS	pY(-3)	13.4 ± 0.69	8.9
AS**A**EpYTILDPS	pY(-2)	13.4 ± 0.99	7.1
ASF**A**pYTILDPS	pY(-1)	22.8 ± 1.40	25.7
ASFEpY**A**ILDPS	pY(+1)	16.6 ± 1.30	11.6
ASFEpYT**A**LDPS	pY(+2)	31.5 ± 1.1	16.1
ASFEpYTI**A**DPS	pY(+3)	34.5 ± 1.3	18.3
ASFEpYTIL**A**PS	pY(+4)	15.3 ± 1.1	13.7
ASFEpYTILD**A**S	pY(+5)	5.4 ± 0.55	8.2
ASFEpYTILDP**A**	pY(+6)	16.7 ± 1.50	10.3

1029 Residue mutated in bold

1030 The K_D measurement by SPR was performed with a single experiment, the SE denotes
1031 uncertainties of fit to the calculated K_D

1032 The NMR was performed with a single experiment at a fixed CPMG delay, therefore no standard
1033 error can be estimated.
1034

Supplementary Figures and Tables

(a)

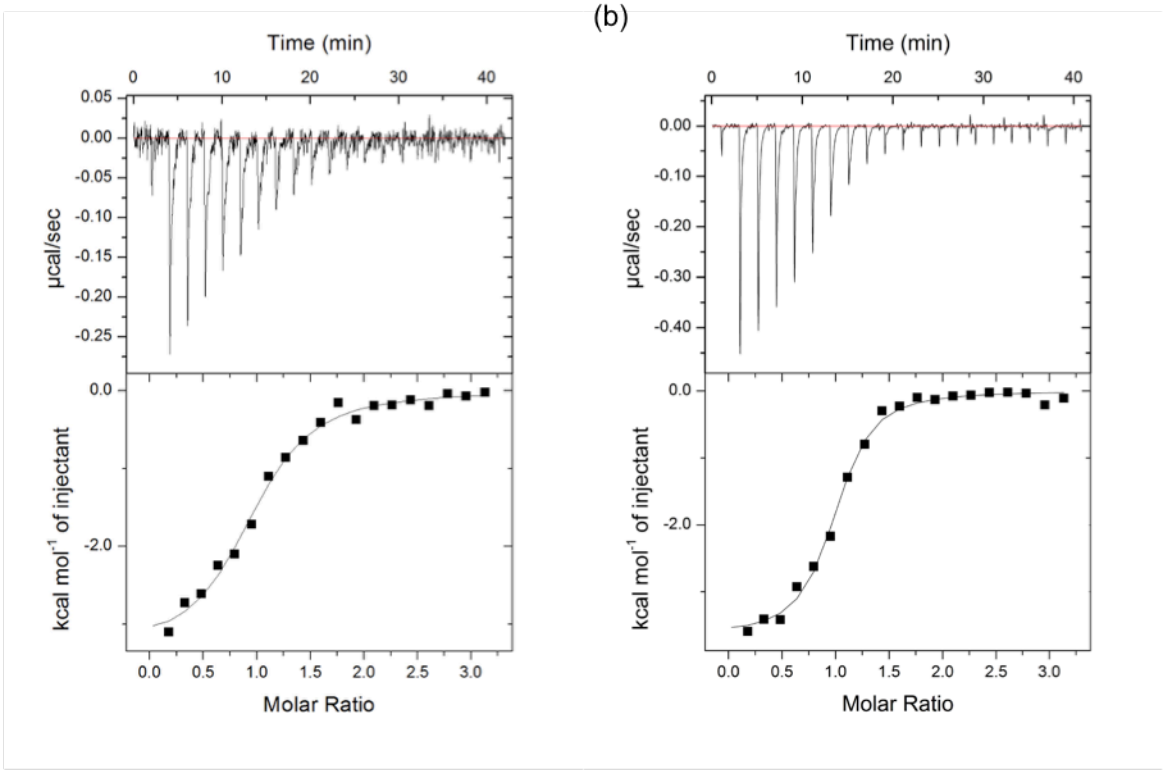

(c)

Peptide	K_D, µM	ΔH, kcal/mol	-TΔS, kcal/mol	ΔG, kal/mol	n
EpoR_pY426†	4.8 ± 0.8	-3.3 ± 0.12	-3.9 ± 0.2	-7.3 ± 0.10	0.96 ± 0.03
GHR_pY595‡	1.6 ± 0.2	-3.6 ± 0.08	-4.2 ± 0.1	-7.9 ± 0.09	0.96 ± 0.01

† EpoR_pY426, ASFEpYTILDPS-amide
‡ GHR_pY595, PVPDpYTSIHIV-amide

Figure S1. Biophysical characterisation of the interactions between SBC and phosphorylated substrate peptides

ITC measurement of (a) the EpoR_pY426 peptide and (b) GHR_pY595 peptide binding to the SOCS2-EloB-EloC ternary (SBC) complex at 298K. (c) ITC binding data for phosphorylated substrate peptides. Values reported are the mean ± s.e.m. from one measurement.

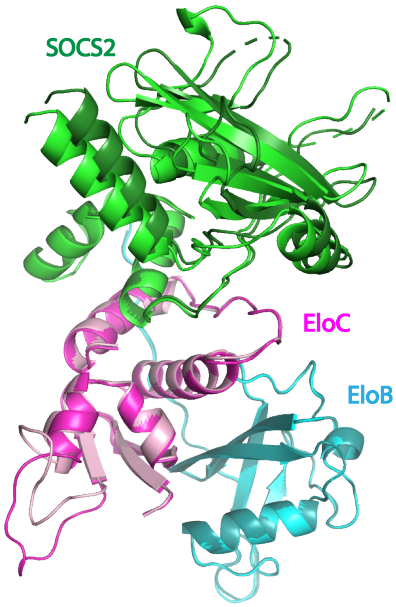

Figure S2. The hinge motion of SOCS2

Superposition of the two protomers from SBC-GHR structure via EloB (cyan and blue) backbone atom alignment. A hinge motion of SOCS2 (green and dark green) is observed.

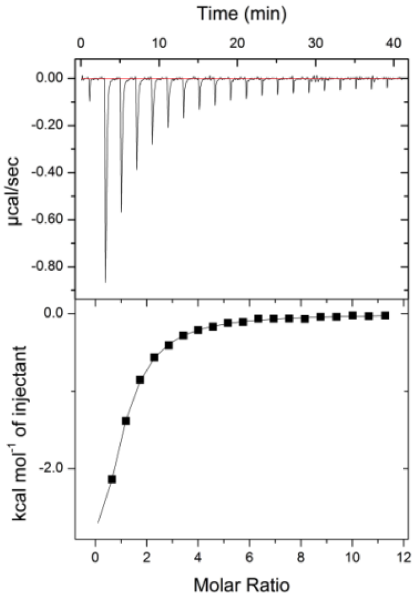

K_D (µM)	42 ± 1.6
ΔG (kcal/mol)	-5.98 ± 0.02
ΔH (kcal/mol)	-5.41 ± 0.25
-TΔS (kcal/mol)	-0.57 ± 0.25
Stoichiometry	0.80 ± 0.03

Figure S3. Biophysical characterization of the interaction between SBC and phosphate 3

ITC measurement was carried out at 298K. Values reported are the mean ± s.e.m. from one measurement.

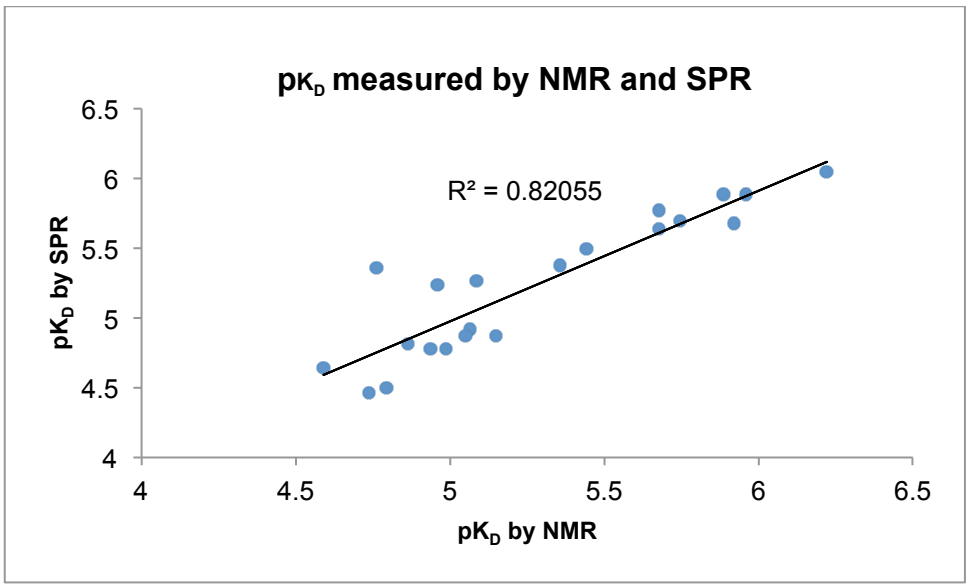

1060

1061 **Figure S4. Correlation of binding affinity of the alanine peptide library measured by**
1062 **^{19}F-NMR and SPR technique**

1063

1064

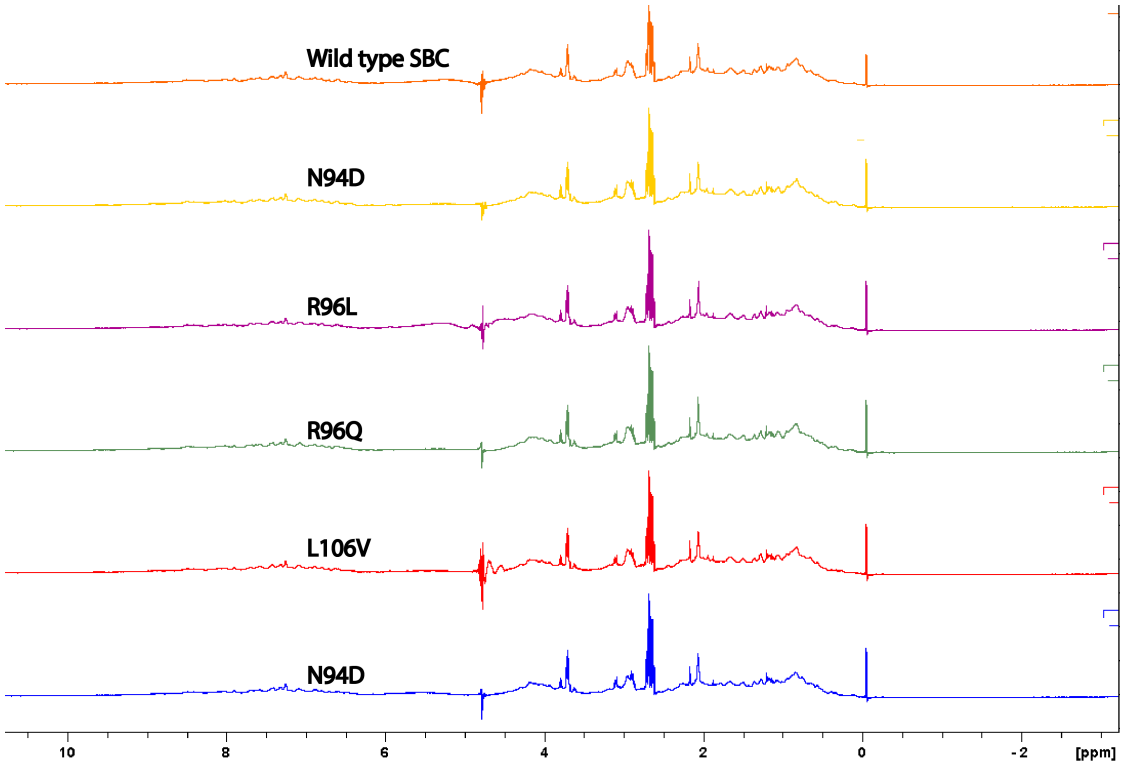

1065

1066 **Figure S5. The protein folding of SNPs containing SOCS2 confirmed by ^{1}H 1D NMR**

1067